Activated Graphene Oxide-Calcium Alginate Beads for Adsorption of Methylene Blue and Pharmaceuticals

Authors: Burcu Gunes[a], Yannick Jaquet[b], Laura Sánchez[c], Rebecca Carrocera [c], Declan McGlade[a], Brid Quilty[a], Anne Morrissey[d], Zahra Gholamvand[a], Kieran Nolan[e], Jenny Lawler[a]

[a] School of Biotechnology and DCU Water Institute, Dublin City University, Glasnevin, Dublin 9, Ireland. Ph: +353 01 700 5787 email: jenny.lawler@dcu.ie

[b] School of Biotechnology , Dublin City University and University of Applied Sciences and Arts Western Switzerland, Glasnevin, Dublin 9, Ireland.

[c] School of Biotechnology, Dublin City University and University of Oviedo, Glasnevin, Dublin 9, Ireland.

[d] School of Mechanical and Manufacturing Engineering and DCU Water Institute, Dublin City University, Glasnevin, Dublin 9, Ireland.

[e] School of Chemical Sciences and DCU Water Institute, Dublin City University, Glasnevin, Dublin 9, Ireland.

Abstract

The remarkable adsorption capacity of graphene derived materials has prompted their examination in composite materials suitable for deployment in treatment of contaminated waters. In this study, crosslinked calcium alginate – graphene oxide beads were prepared and activated by exposure to pH 4 by using 0.1M HCl. The activated beads were investigated as novel adsorbents for the removal of organic pollutants (Methylene Blue dye and the pharmaceuticals Famotidine and Diclofenac) with a range of physicochemical properties. Effects of initial pollutant concentration, temperature, pH and adsorbent dose were investigated and kinetic models were examined for fit to the data. Maximum adsorption capacities q_{max} obtained were 1334, 35.50 and 36.35 mg g^{-1} for the uptake of Methylene blue, Famotidine and Diclofenac respectively. The equilibrium adsorption had an alignment with Langmuir isotherms while the kinetics were most accurately modelled using a pseudo- first – order and second order models according to the regression analysis. Thermodynamic parameters such as ΔG°, ΔH° and ΔS° were calculated and the adsorption process was determined to be exothermic and spontaneous.

Keywords: Adsorption; Graphene oxide; Methylene blue; Pharmaceuticals; Kinetics, Isotherms and Thermodynamics

 doi:10.20944/preprints202009.0562.v1

1 Introduction

Micropollutants such as pharmaceuticals, personal care products, surfactants and pesticides [1] as well as synthetic dyes [2] have been found virtually ubiquitously in environmental matrices over the past decade. One major source of organic micropollutants are effluents from wastewater treatment plants (WWTPs) since most of these emerging contaminants are poorly biodegradable [3]. In addition, the hazards presented for human health and the ecosystem of thousands of trace contaminants in a "cocktail effect" is not yet well understood, although advances in effect based biomonitoring aim to address this [4], [5].

Methylene blue (MB) is a heterocyclic aromatic chemical dye used in textile, paper and cosmetic industries [6]. It is not highly toxic but has significant adverse impacts on aquatic ecosystems [2], retarding photosynthetic activity of aquatic plants by affecting the light penetration, consuming dissolved oxygen or isolating metal ions producing microtoxicity to organisms [7]–[10]. It can also be harmful to human health, causing heart rate increase, nausea and vomiting [11]. Methylene blue is widely used as an indicator pollutant to demonstrate the efficiency of novel adsorbent materials in the literature. Famotidine (FMTD) is a histamine H_2-receptor antagonist used for treating gastroesophageal reflux disease and Zollinger-Ellison syndrome [12]. Famotidine has been shown to persist in WWTP effluents [13]–[15]. Diclofenac (DFC) is a non-steroidal anti-inflammatory drug prescribed to reduce inflammation, pain and dysmenorrhea; consumption is associated with serious dose-dependent gastrointestinal, renal and hepatic adverse effects, and increases vascular and coronary risks by about 33% [16], [17]. Diclofenac is monitored in European surface waters under the Watch List mechanism for the Water Framework Directive, and has been found almost ubiquitously in wastewater influent, wastewater effluent and surface waters [18]. Diclofenac exposure to trout has been shown to induce severe glomerulonephritis resulting into kidney failure [19] and it has been implicated in the collapse of Asian vulture populations [20].

Removal of micropollutants and synthetic dyes using membrane based technologies, ozonation, photolysis, photocatalysis [21]–[23], electrolysis, Fenton [24], photo-Fenton oxidation and electrochemical oxidation [25] have been extensively investigated in the literature. In particular, adsorption technology holds a lot of advantages such as easy operation, fast decolorization and chemical oxygen demand removal efficiency, however the

 doi:10.20944/preprints202009.0562.v1

main limitation of adsorption technology is the low and non-selective adsorption capacity of traditional adsorbents. Enhancement of adsorption capacity by increasing surface area and optimising pore size has received much research attention [26]–[31].

Graphene based materials have received increasing attention as potential candidates for composite preparation due to high specific surface area and adsorption capacity. Graphene oxide (GO) is a two dimensional complex of carbon atoms decorated with a multitude of oxygen containing functional groups densely packed in a honeycomb framework [32]. GO has unique properties such as large theoretical surface area, high thermal and chemical stability, high conductivity and good mechanical flexibility [33], showing a great potential as an adsorbent for removal of pharmaceuticals [34] heavy metals [35], [36] or dyes [37]. In this study, to stabilize the GO [38], maximise the ease of recovery, and improve the adsorption capacity, GO was incorporated into an alginate matrix (an anionic polysaccharide used in paints, inks or pharmaceuticals). Alginate forms a hydrogel when mixed with divalent cations, like Ca^{2+}, giving good mechanical properties. Acid-activation of the beads provides an enhancement in the surface area including micro and mesopores [39], [40]. In fact, adsorption capacity of GO-montmorillonite/sodium alginate beads was recently investigated [41].

In this work, acid activated (0.1 M HCl pH 4) adsorption capacity of calcium alginate graphene oxide beads were evaluated as novel adsorbent for MB, FMTD and DFC removal. In addition, influence of initial pollutant concentration, adsorbent dose, adsorption temperature and pH on adsorption capacity was investigated along with examination of kinetic and thermodynamic modelling of the reactions.

2 Materials and Methods

2.1 Materials

Graphite flakes (GF) were purchased from Asbury Carbons. Diclofenac sodium (DFC, 99%), Famotidine (FMTC), Methylene blue (MB) and alginic acid sodium salt (Na-Alg) were purchased from Sigma Aldrich. Calcium chloride dihydrate, sodium hydroxide, potassium permanganate and absolute ethanol were purchased from Fischer Chemicals. Sulphuric acid (H_2SO_4, 95-98%) and Hydrogen peroxide (H_2O_2, 30%) was purchased from Merck Millipore. Hydrochloric acid (37%) was provided by Acros Organics.

Preprints (www.preprints.org) | NOT PEER-REVIEWED | Posted: 24 September 2020 doi:10.20944/preprints202009.0562.v1

2.2 Methods

2.2.1 Preparation of Graphene oxide (GO) Solution and Ca-Alg2/GO Beads

GO was prepared according to modified Hummer's method [42]. In this method, expanded graphite is derived from the graphite flasks were treated with H_2SO_4 to be mixed with H_2O_2 in order to produce GO particles. To establish the concentration, 1 g of GO suspension was spread in a dried, weighed beaker, dried overnight at 60°C and weighed again, and the concentration was then adjusted to 1% GO in DI water on a dry mass basis. The details of the method and Ca-Alg2/GO beads preparation is given in supplementary data (S.2).

2.3 Acid Activation of the Beads activations

Beads for activation were placed into 600 mL beakers of DI water adjusted to pH4 using 0.1M HCl, which were agitated for 3 hours. Afterwards, the beads were collected, rinsed three times with 300 mL of DI water and stored in a closed bottle at RT.

2.4 Characterization

The surface morphological structure of the beads was examined using scanning electron microscopy (SEM) analysis using a Hitachi 3400 SEM, following gold coating. Functional groups of the GO sheets as well as of the Ca-Alg2 and Ca-Alg2/GO beads was identified by Fourier transform infrared spectroscopy. In addition, the GO used for the bead's preparation was characterised by X-Ray Diffraction and Raman spectroscopy (S.5).

2.5 Adsorption Measurements

All adsorption measurements were carried out in 250 mL flasks with 0.05 g adsorbent (Ca-Alg_2, Ca- Alg_2/GO5, Ca-Alg_2/GO10 or Ca-Alg_2/GO20 dried beads), over 24 hours on a shaker table operating at 125 rpm at room temperature (22°C), unless otherwise specified. Equilibrium for all pollutants was established by 24 hours. 75 mL of pollutant solution at a concentration of 10 mg L^{-1} was added in each case, with a pH of 7 for MB and FMTD and a pH of 2 for DFC, unless otherwise specified. Pollutant concentration was determined using a UV-VIS spectrophotometer (Varian) at a wavelength of 660, 286 and 274 nm for MB, FMTD and DFC, respectively. Experiments were carried out in triplicate and the average value reported along with the error bars represent the standard deviation.

Preprints (www.preprints.org) | NOT PEER-REVIEWED | Posted: 24 September 2020 doi:10.20944/preprints202009.0562.v1

2.5.1 Initial Pollutant Concentration

The initial pollutant concentrations tested were 10, 100, 500, 1000 mgL^{-1} for MB, 10, 25, 100, 250 mgL^{-1} for FMTD and 1, 5, 10, 25 mgL^{-1} for DFC. The absorbed amount at equilibrium (q_{eq} ($mg\ g^{-1}$)) was calculating using Eq 1:

$$q_{eq} = \frac{(C_0 - C_{eq}) \cdot V}{m_{ads}} \quad \text{(Eq.1)}$$

where C_0 ($mg\ L^{-1}$) is the initial pollutant concentration, C_{eq} ($mg\ L^{-1}$) the equilibrium pollutant concentration, V (L) the solution volume and m_{ads} (g) the adsorbent mass.

2.5.2 Adsorbent dose

The effect of the adsorbent dose was studied using 0.01, 0.025, 0.05 and 0.1 g of Ca-Alg_2, Ca-Alg_2/GO5, Ca-Alg_2/GO10 or Ca-Alg_2/GO20 dried beads.

2.5.3 pH

The adsorption was performed at pH 7, 9, 10 and 11 for MB and FMTD whereas the adsorption for DFC was at pH 2, 3.5, 5 and 7.

2.5.4 Temperature

The influence of the temperature was studied by performing the adsorption process at 4, 22 and 30°C.

2.5.5 Thermodynamics

The thermodynamic parameters of adsorption were determined at 4, 22 and 30°C in order to evaluate the feasibility and the spontaneous nature of the adsorption. Adsorption distribution coefficient K_d is calculated using Eq 2:

$$K_d = \frac{C_0 - C_{eq}}{C_{eq}} \quad \text{(Eq. 2)}$$

Where C_0 ($mg\ L^{-1}$) is the initial concentration of the solution and C_{eq} ($mg\ L^{-1}$) the equilibrium concentration in solution. A plot of $\ln(K_d)$ versus 1/T gives a straight line where the enthalpy change $\Delta H°$ ($J \cdot mol^{-1}$) and the entropy change $\Delta S°$ ($J \cdot K^{-1} \cdot mol^{-1}$) can be calculated using (Eq. 3):

$$ln(K_d) = \frac{\Delta S°}{R} - \frac{\Delta H°}{RT} \quad \text{(Eq. 3)}$$

Where R is the ideal gas constant (8.345 $Jmol^{-1}K^{-1}$) and T (K) is the temperature of the solution during the adsorption process. The standard Gibbs free energy change was obtained from Eq 4:

$$\Delta G° = \Delta H° - T\Delta S° \quad \text{(Eq. 4)}$$

Preprints (www.preprints.org) | NOT PEER-REVIEWED | Posted: 24 September 2020 doi:10.20944/preprints202009.0562.v1

2.5.6 Kinetics

Kinetic parameters were studied using 0.05 g of Ca-Alg$_2$, Ca-Alg$_2$/GO5, Ca-Alg$_2$/GO10 or Ca-Alg$_2$/GO20 dried beads. The three most common models were examined as to their fit to the experimental data [43].

The adsorbate capacity q_t (mg g^{-1}) at time t was calculated using Equation 5:

$$q_t = \frac{(C_0 - C_t) \cdot V}{m_{ads}} \quad \text{(Eq. 5)}$$

Where C_0 (mgL^{-1}) is the initial concentration, C_t (mgL^{-1}) the concentration at time t, V (L) the volume of pollutant solution and m_{ads} (g) the adsorbent mass.

The linearized- integral form of the pseudo-first –order Lagergren equation is given by Eq. 6:

$$ln(q_{eq} - q_t) = ln(q_{eq}) - k_1 \cdot t \quad \text{(Eq. 6)}$$

where k_1 (min^{-1}) is the Lagergren rate constant, q_{eq} (mg g^{-1}) is the maximum adsorbed amount at equilibrium, and q_t (mg g^{-1}) is the amount of adsorption at time t (min). The values of k_1 and q_{eq} were determined from the intercept and the slope of a plot of $\ln(q_{eq} - q_t)$ versus t.

The linearized integral form of the pseudo-second-order model is shown in Eq. 7:

$$\frac{t}{q_t} = \frac{1}{k_2 \cdot q_{eq}^2} - \frac{1}{q_{eq}} \cdot t \quad \text{(Eq. 7)}$$

Where k_2 (g·mg^{-1}·min^{-1}) is the pseudo second-order rate constant of adsorption. The parameters k_2 and q_{eq} were determined from the intercept and the slope of a plot of t/q_t versus t.

The intraparticle diffusion model is represented in Eq. 8:

$$q_t = k_{ip} \cdot t^{1/2} + C_{ip} \quad \text{(Eq. 8)}$$

Where k_{ip} (mg g^{-1}·min$^{-0.5}$) is an intraparticle diffusion rate constant and C_{ip} (mg g^{-1}) is related to the thickness of the diffusion boundary layer. These parameters were obtained from a plot of q_t versus $t^{1/2}$.

2.5.7 Adsorption isotherms

The Langmuir model and the Freundlich model were examined for their utility in describing the adsorption process. The Langmuir equation is detailed in Eq. 9: [44]

$$q_{eq} = q_{max} \cdot \frac{C_{eq}}{k_L + C_{eq}} \quad \text{(Eq. 9)}$$

Where q_{max} (mg g^{-1}) is the maximum adsorption capacity corresponding to complete monolayer coverage, C_{eq} (mgL^{-1}) is the concentration at equilibrium in the solution and k_L (Lg^{-1}) is a constant related to adsorption capacity and energy of adsorption.

Preprints (www.preprints.org) | NOT PEER-REVIEWED | Posted: 24 September 2020 doi:10.20944/preprints202009.0562.v1

The Freundlich equation is an empirical model based on the adsorption on a heterogeneous surface [45] is given in Eq. 10:

$$q_{eq} = k_F \cdot C^n \quad (10)$$

Where k_F (L·g^{-1}) and n (-) are the Freundlich constants, indicating the adsorption capacity and the adsorption intensity, respectively. In order to determine the Langmuir and Freundlich constants, Excel Solver was used to fit the adsorption isotherm models with the experimental data. The sum of squared differences between experimental q_{eq} and calculated q_{eq} was minimized by changing the constants of the models with the solver to find the best non-linear regression.

2.6 Desorption Studies

After the concentration at equilibrium was determined, the beads were removed from the solution and were washed three times with DI water. The desorption of pollutants from the beads was examined by using three different desorption systems, 0.1 M HCl, 1 M NaCl and Ethanol 1% v/v. The desorption process was carried out in 250 mL conical flasks with 75 mL of desorption solution at RT. The conical flasks were agitated for 24 hours at 125 rpm. Then, the final concentration in solution was determined using UV-VIS and the percentage desorption calculated using Eq. 11:

$$\text{Desorption} = \frac{(q_{eq,a} - q_{eq,d})}{q_{eq,a}} \cdot 100 \quad (\text{Eq } 11)$$

Where $q_{eq,d}$ (mg g^{-1}) is the adsorbed amount at equilibrium after 24 hours of desorption, and $q_{eq,a}$ (mg g^{-1}) is the adsorbed amount at equilibrium after 24 hours of adsorption.

Preprints (www.preprints.org) | NOT PEER-REVIEWED | Posted: 24 September 2020 doi:10.20944/preprints202009.0562.v1

3 Results and Discussion

3.1 Characterization of Beads

SEM analysis was carried out in order to characterize the morphological structure of the beads and the results are given Figure 1 and Figure 2 at 500 and 5000 magnification respectively. In addition, the images of the wet and dry beads were given in supplementary data file (S3).

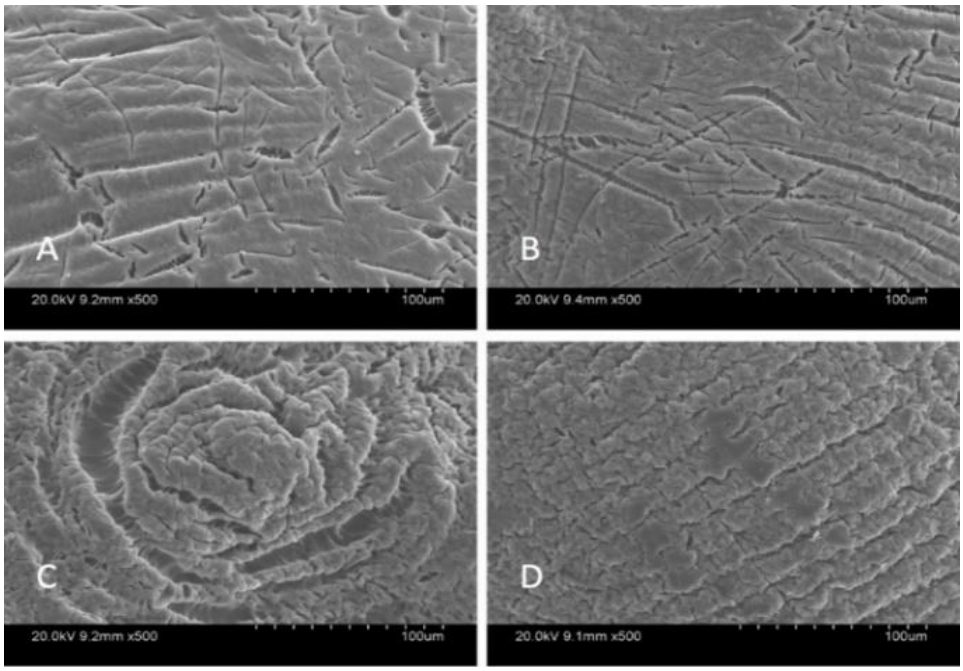

Figure 1 SEM images of beads at x500 magnification: Ca-Alg$_2$ (A), Ca-Alg$_2$/GO5 (B), Ca-Alg$_2$/GO10 (C), Ca-Alg$_2$/GO20 (D)

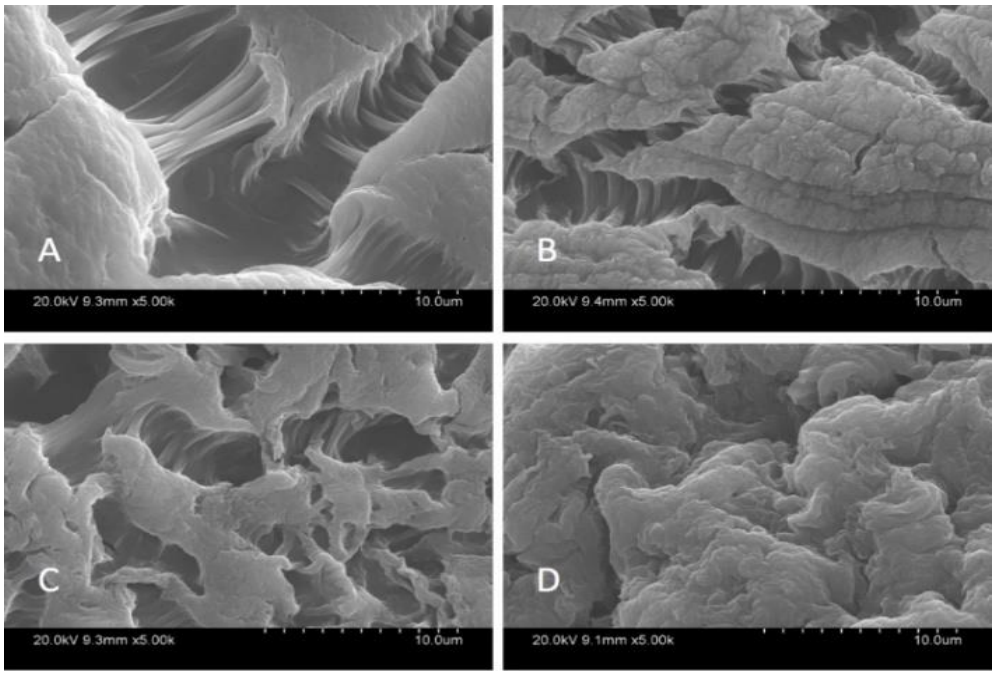

Figure 2 SEM images of beads at 5000x; Ca-Alg2 (A), Ca-Alg2/GO5 (B), Ca-Alg2/GO10 (C), Ca-Alg2/GO20 (D)

 doi:10.20944/preprints202009.0562.v1

The SEM images showed that increased graphene oxide concentration altered the morphological structure of the beads by providing an increased porosity and roughness. Due to that increase beads had a greater surface available for interactions between adsorbate and adsorbent. The Ca-Alg_2/GO20 was typically carbonaceous with similarities to activated carbon structure. The FTIR spectrum of GO sheets, Ca-Alg2 and Ca-Alg2/GO beads is given in S4. No significant difference was observed between Ca-Alg2 and Ca-Alg2/GO beads as the functional groups of the alginate overlap with GO.

Preprints (www.preprints.org) | NOT PEER-REVIEWED | Posted: 24 September 2020 doi:10.20944/preprints202009.0562.v1

3.2 Effect of Operating Parameters on the Adsorption

3.2.1 Contact Time

The effect of the contact time on q_t was examined by taking samples over 24 hours. The average of the results obtained for the adsorption of MB, FMTD and DFC given in Figure 3 A, B and C respectively.

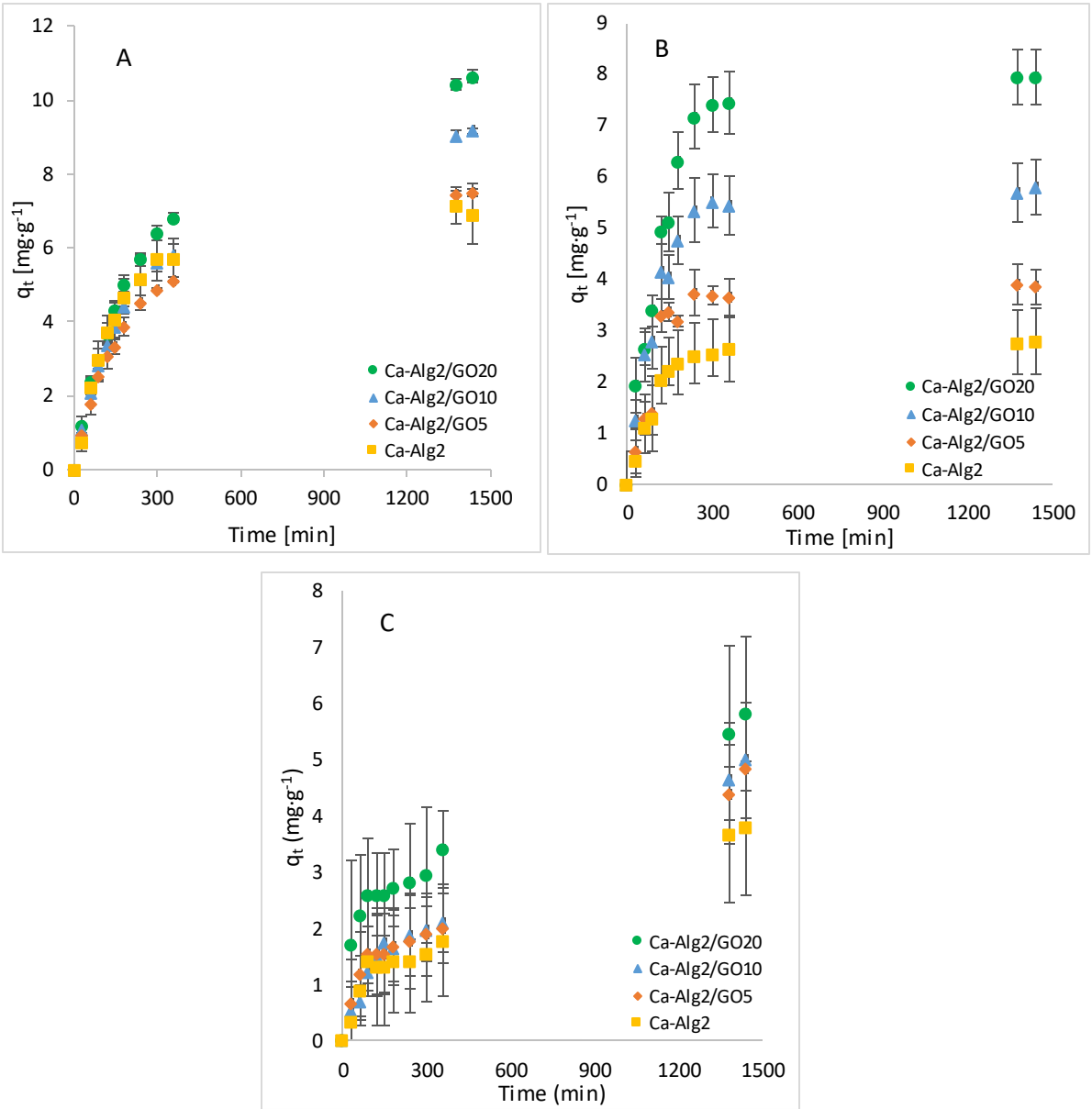

Figure 3 Effect of the contact time on q_{eq} of A. MB, B. FMTD and C. DFC

The adsorption gradually increased with the contact time and slowed down progressively to reach an equilibrium after 24 h. An increased adsorbate capacity was achieved with an increased concentration of GO in the composites. Ca-Alg$_2$/GO20 beads were the most

Preprints (www.preprints.org) | NOT PEER-REVIEWED | Posted: 24 September 2020 doi:10.20944/preprints202009.0562.v1

efficient for the adsorption of each compound as expected. For adsorption of MB, Ca-Alg2/GO10 and Ca-Alg2/GO20 beads had a significant improvement in the adsorbate capacity by increasing it from 6.91±0.83 mg g^{-1} to 9.18±0.08 and 10.63±0.17 mg g^{-1} in comparison to Ca-Alg2 (control) with the *p* values of 0.034 and 0.023 respectively. For adsorption of FMTD, Ca-Alg2/GO composites regardless the level of GO had a significant improvement (p <0.05) in adsorbate capacity from 2.78±0.34 mg g^{-1} reaching the maximum of 7.95±0.54 mg g^{-1} with Ca-Alg2/GO20. On the other hand, for adsorption of DFC, no significant enhancements were seen (high level of error bars) which was attributed to molecular limitations of DFC.

3.2.2 Pollutant Concentration

The effect of the different concentration of methylene blue, famotidine and diclofenac on the adsorption density (q_{eq}) and the percentage removal are shown in Figures 4-6.

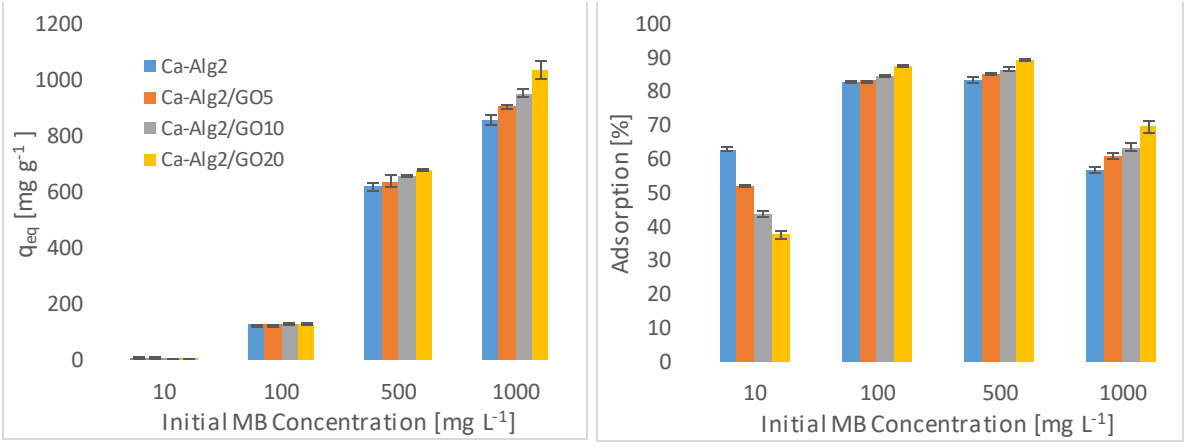

Figure 4 Effect of the initial MB concentration on q_{eq} and adsorption percentage

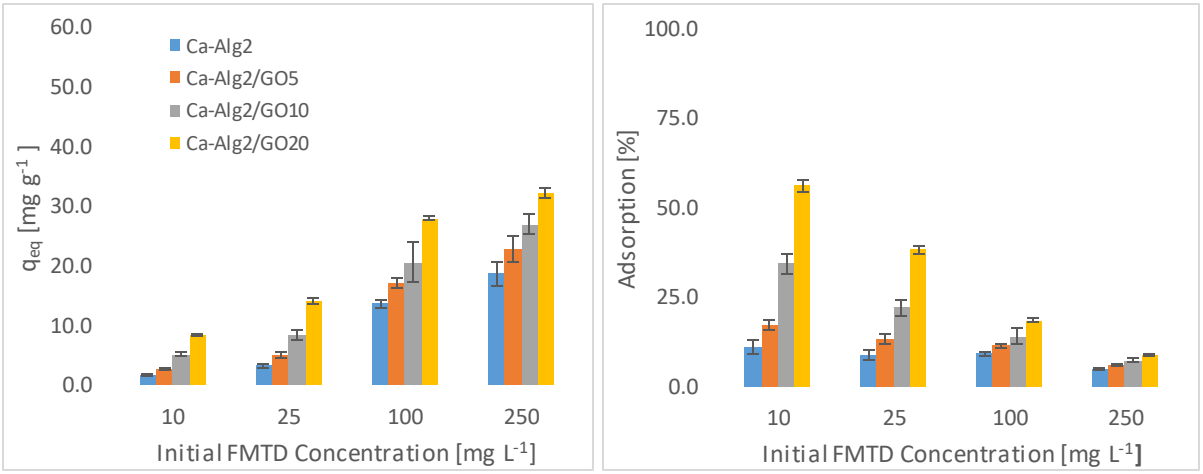

Figure 5 Effect of the initial concentration of FMTD on q_{eq} and adsorption percentage

Preprints (www.preprints.org) | NOT PEER-REVIEWED | Posted: 24 September 2020 doi:10.20944/preprints202009.0562.v1

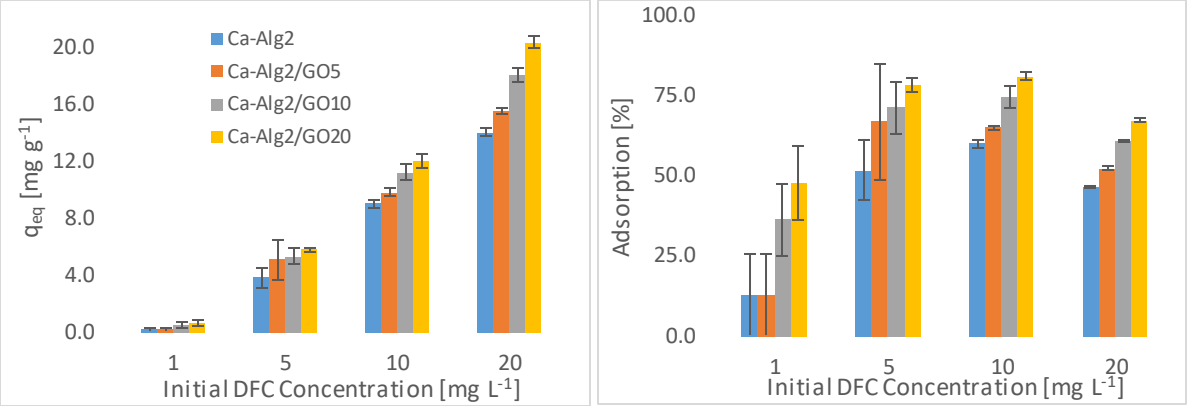

Figure 6 Effect of the initial concentration of DFC on q_{eq} and adsorption percentage

Higher levels of adsorbed amount of pollutant at equilibrium (q_{eq}) were achieved with an increased GO level in the composites when the initial concentration of the pollutants (MB, FMTD and DFC) was higher. For the highest initial pollutant concentrations, which was 1000, 250 and 20 mgL^{-1} for MB, FMTD and DFC respectively, all Ca-Alg2/GO beads (regardless the GO level) had a significant increase in q_{eq} value (p<0.05) for DFC whereas only Ca-Alg2/GO10 and Ca-Alg2/GO20 beads showed a significant improvement on q_{eq} value of MB and FMTD with regards to Ca-Alg2 beads. The greatest enhancements were achieved with Ca-Alg2/GO20 beads from 856.4±16.8 to 1036.2±30.7mg g^{-1} (p:0.022) for MB, from 18.6±1.9 to 32.2±0.8 mg g^{-1} (p:0.004) FMTD and from 14.1±0.329 to 20.4±0.427 mg g^{-1} (p:0.0001) for DFC for the highest pollutant concentrations.

Ca-Alg2/GO20 beads had the highest adsorption percentage for each pollutant as expected. The highest adsorption percentages were found to be 89.4±0.25, 56.0±1.7 and 80.9±1.35 for MB, FMTD and DFC respectively which were significantly higher than the corresponding control.

3.2.3 Adsorbent Dose

The effect of the adsorbent dose on adsorption density and adsorption percentage was observed by using four different masses of beads varied from 0.01 to 1.0. The adsorption density (q_{eq}) for four different types of beads and percentage adsorption of MB, FMTD and DFC on Ca-Alg2/GO20 beads are given Figure 7, 8 and 9 respectively as function of amount of adsorbent.

Preprints (www.preprints.org) | NOT PEER-REVIEWED | Posted: 24 September 2020 doi:10.20944/preprints202009.0562.v1

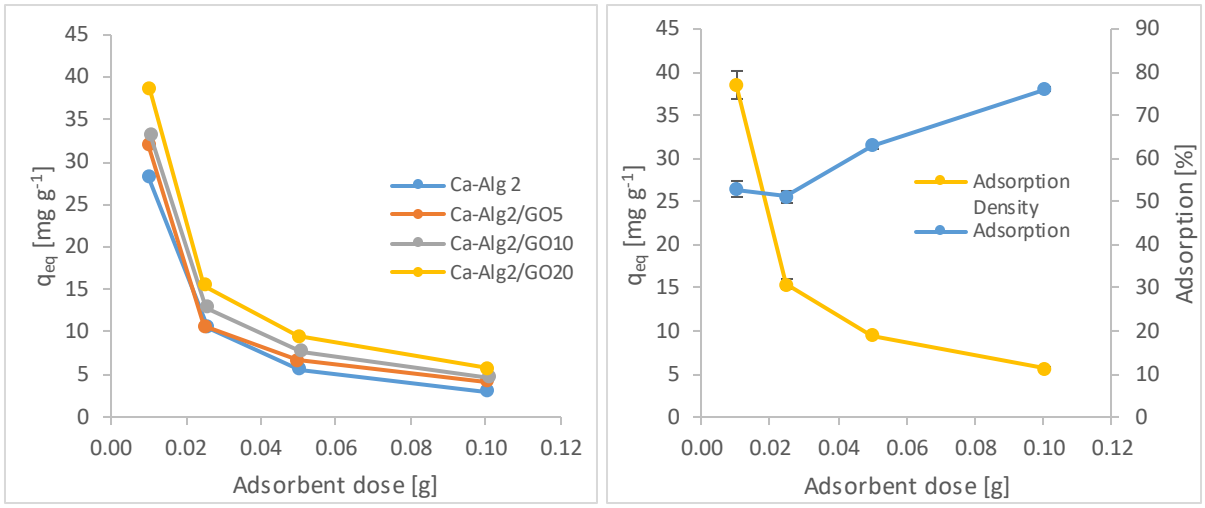

Figure 7 Effect of the adsorbent dose on qeq MB

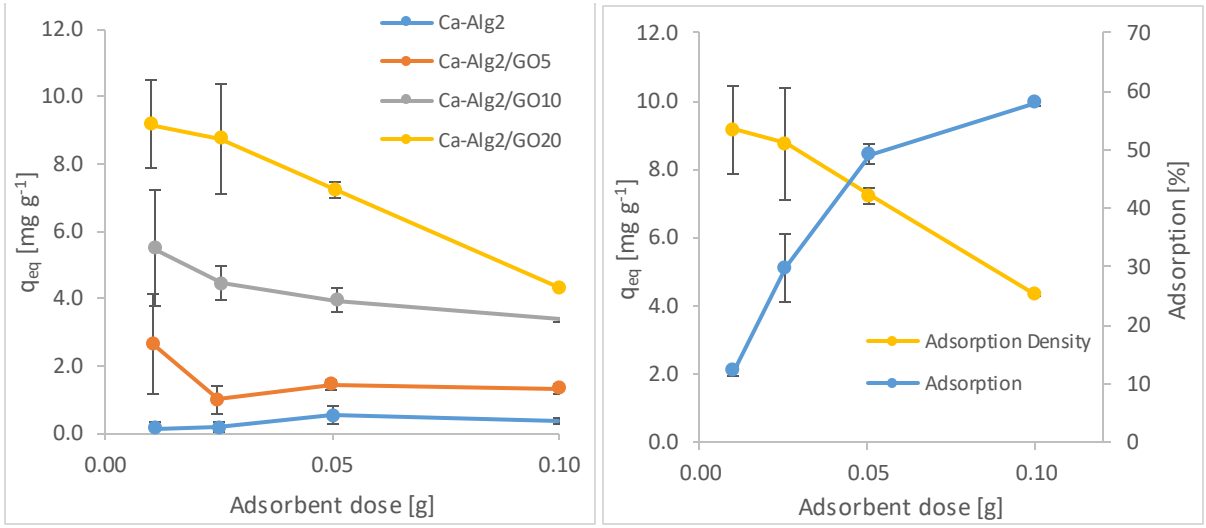

Figure 8 Effect of the adsorbent dose on qeq FMTD

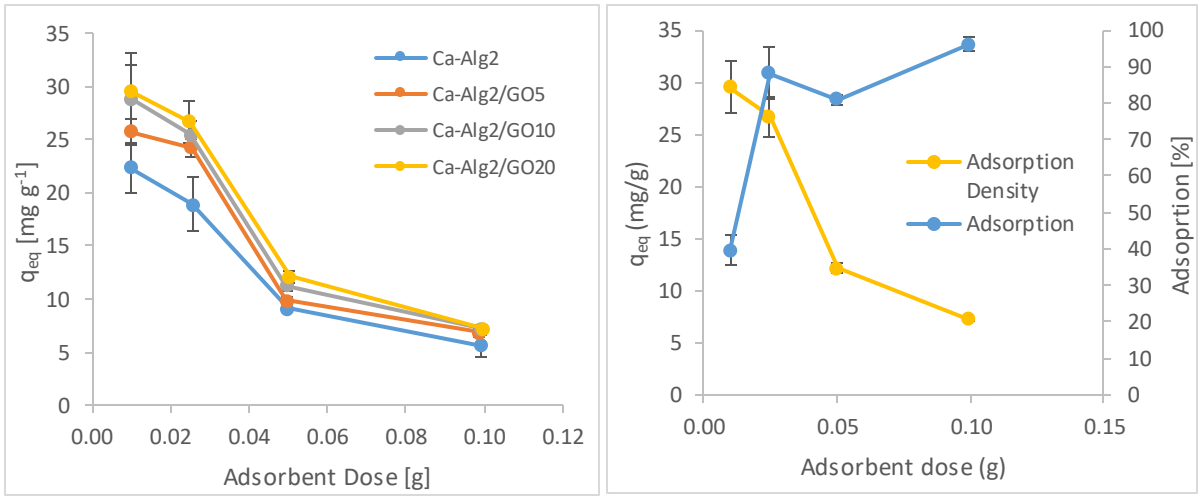

Figure 9 Effect of the adsorbent dose on qeq DFC

Preprints (www.preprints.org) | NOT PEER-REVIEWED | Posted: 24 September 2020 doi:10.20944/preprints202009.0562.v1

A decreased adsorption density has been observed with the increased adsorbent dose regardless of the type of beads and of pollutant. On the other hand, adsorption percentage increased significantly (p<0.05) when Ca-Alg2/GO20 beads used from 52.9±1.7 to 76±0.4% for MB, from 12.2±0.9 to 58.2±0.5% for FMTD and from 39.7±4.1 to 96.1±1.7% for DFC due to increase in adsorbent dose from 0.1 to 1.0. On the contrary, adsorption density decreased significantly (p<0.05) from 38.9±1.6 to 5.7±0.1 mg g^{-1} for MB, from 9.2±1.3 to 4.3±0. mg g^{-1} for FMTD and from 29.5±2.5 to 7.2±0.1 mg g^{-1} for DFC due to increase in adsorbent dose from 0.1 to 1.0. The reduction in the adsorption density was attributed to a lower quantity adsorbed per unit weight of the adsorbent, causing the presence of unsaturated adsorption sites [46] when the adsorbent dose is increased [47], [48]. Ca-Alg_2/GO20 beads were shown to exhibit significantly better adsorption than Ca-Alg_2 beads.

3.2.4 pH

The impact of the pH on adsorption was observed by using four pH values (7, 9, 10, 11.5 for cationic molecules and 2, 3.5, 5 and 7 for anionic molecules). The average of the results obtained for the adsorption of MB, FMTD and DFC are shown in the figures below (Figure 9 A,B and C).

Preprints (www.preprints.org) | NOT PEER-REVIEWED | Posted: 24 September 2020 doi:10.20944/preprints202009.0562.v1

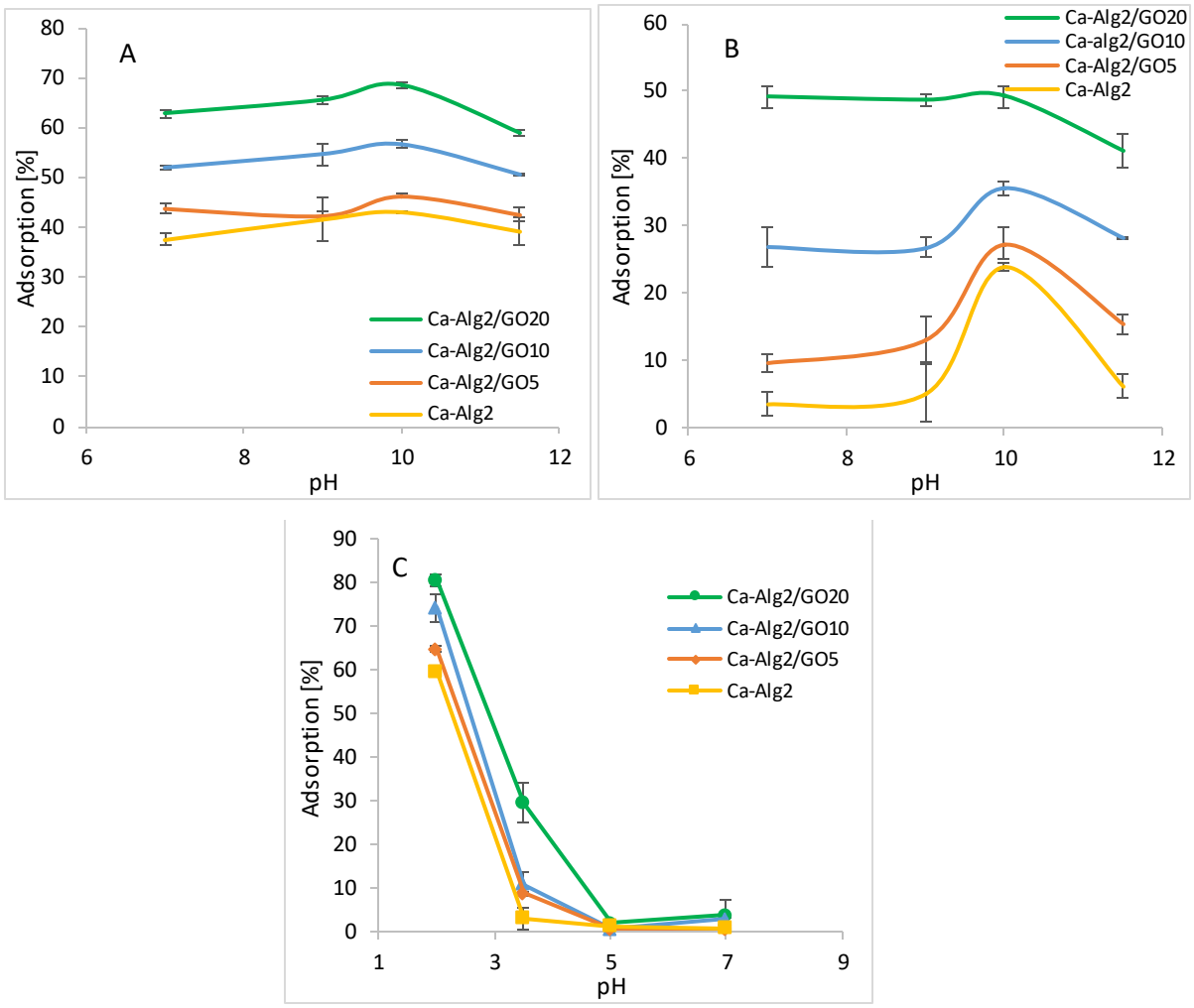

Figure 10 Effect of the pH on qeq A. MB, B. FMTD, C. DFC

The adsorption percentage of MB at pH 7 found as 62.9±0.75% which slightly increased up to 68.6±0.7% at pH10 and attained a maximum value (Figure 10 A) when Ca-Alg2/GO20 beads were used. Similarly, the highest MB adsorptions were obtained at pH 10 with other beads. The adsorption percentage of FMTD has shown a peak at pH 10 with for different types of beads with the maximum of 49.2±1.6% (Figure 10 B) when Ca-Alg2/GO20. Therefore, adsorption of cationic molecules, MB and FMTD, increases with higher pH solutions until they reach a pH of 10, then it starts to decrease. This observation can be explained by looking at the pK_a values for the analytes and Ca-Alg2/GO20 beads. At pH 10 FMTD is in the neutral form, since its pK_a value is 6.98 [49], and possess lower water solubility thereby enhancing the adsorption process at this pH. MB still possesses a positive charge at pH 10 however GO has an increased negative charge at pH 10 since the phenolic groups of GO are now becoming ionised (GO pK_a = 4.3; 6.6; 9.8 all acid groups and 50% of GO phenolic groups will be ionised)

Preprints (www.preprints.org) | NOT PEER-REVIEWED | Posted: 24 September 2020 doi:10.20944/preprints202009.0562.v1

[50] enhancing the charge attraction between MB and the adsorbent which explains the larger adsorption capacity between Ca-Alg2/GO20 and Ca-Alg2 in Figure 10 A.

On the other hand, for the anionic molecules, DFC, the highest adsorption percentage was observed as 96.1±1.7% (Figure 10 C) when Ca-Alg2/GO20 beads were used at pH 2. The adsorption percentage showed a sudden drop when the pH level is increased to 3.5 and further increase in pH level had a negative impact on adsorption for four different bead types. The observed decrease in adsorption of diclofenac at higher pH is a consequence of the non-ionised to ionised form of diclofenac (pK_a = 4.0), alginate (pK_a mannuronic = 3.38 and guluronic acid = 3.65 [51]) and GO. At pH 2 the ratio of non-ionised to ionised diclofenac is 100:1 (see Supplementary Data S7) alginate is 45:1 (pK_a 3.65) and GO 200:1. These ratios change at pH 3.5 to 3.16:1, 1.4:1 and 6.3:1 for diclofenac, alginate and GO respectively. Thus, diclofenac, alginate and GO are gaining negative charge and as a consequence repulsion is occurring. Furthermore, as diclofenac becomes negatively charged its water solubility is significantly enhanced consequently reducing adsorption [52], [53].

3.2.5 Temperature

Adsorption studies were performed across three temperatures ranging from 4 to 30°C (4, 22 and 30°C). The average of the results obtained for the adsorption of MB, FMTD and DFC are shown in Figure 11 A, B and C.

Preprints (www.preprints.org) | NOT PEER-REVIEWED | Posted: 24 September 2020 doi:10.20944/preprints202009.0562.v1

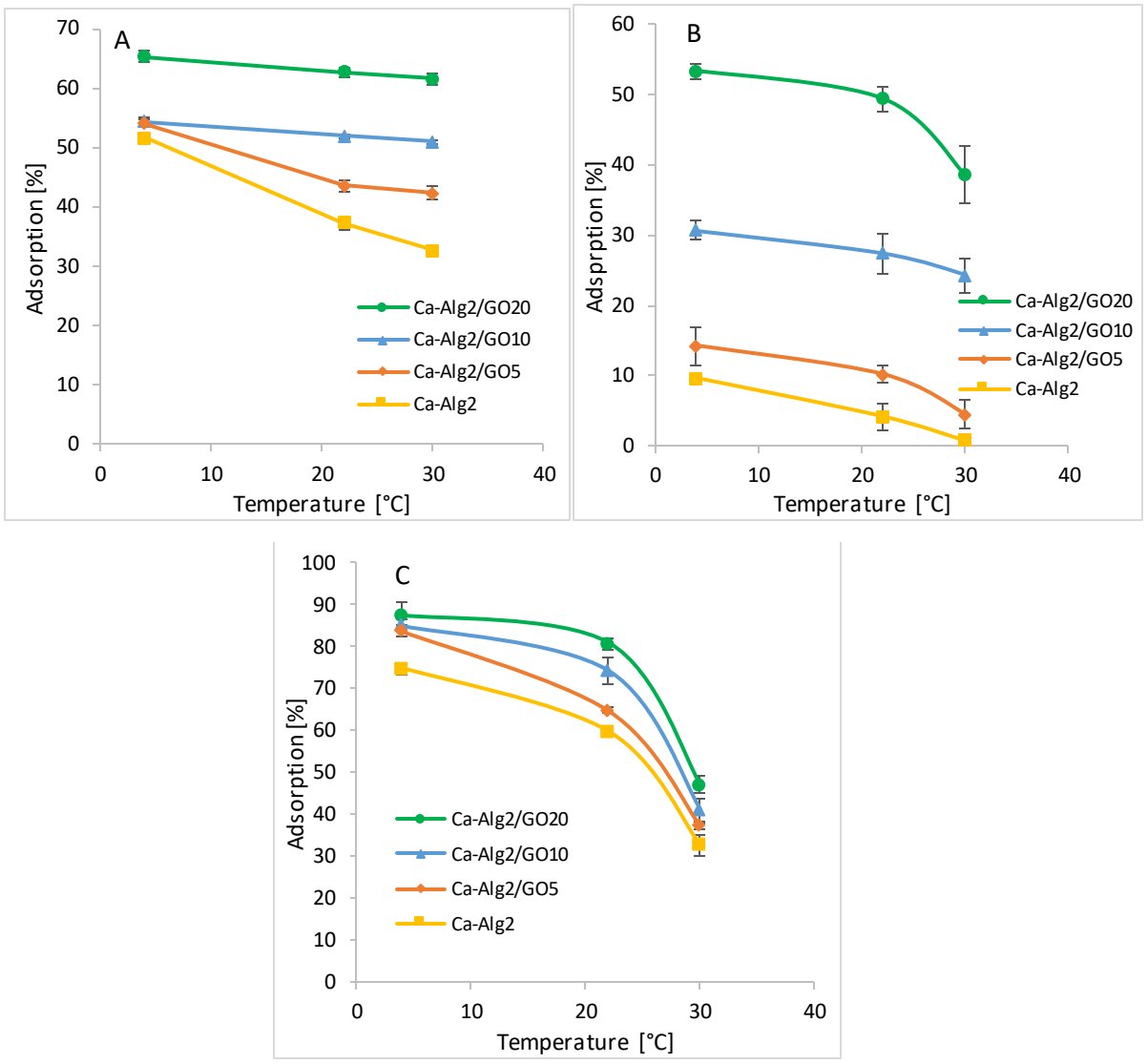

Figure 11 Effect of the temperature on qeq of A. MB, B. FMTD, C. DFC

The coldest temperature (4°C) showed the highest adsorption percentages as 65.3±0.9% (Figure 11 A), 53.3±1.2% (Figure 11 B) and 87.3±3.4% (Figure 11 C) for MB, FMTD and DFC respectively when Ca-Alg2/GO20 beads were used. The adsorption of MB, FMTD and DFC decreased significantly due to stepwise increase in temperature to 22 and 30°C and reached to 61.1±1.0, 38.6±4.0 and 47.1±2.0% respectively under the same conditions. It may be explained by an exothermic adsorption process [56].

Preprints (www.preprints.org) | NOT PEER-REVIEWED | Posted: 24 September 2020 doi:10.20944/preprints202009.0562.v1

3.3 Thermodynamics

Thermodynamic studies were conducted based on the feasibility and the spontaneous nature of adsorption [43]. Distribution coefficient for the adsorption K_d, enthalpy change $\Delta H°$, entropy change $\Delta S°$ and Gibbs free energy change $\Delta G°$ were calculated using Equations 2, 3 and 4. The results are given in the Tables 1, 2 and 3.

A significant decrease ($p<0.05$) in the distribution coefficient (K_d) was observed in all cases when the adsorption temperature was increased from 4 to 30°C indicating that better adsorption at lower temperatures. For example, K_d value for adsorption of MB, FMTD and DFC on Ca-Alg2/GO20 beads decreased from 1.88 to 1.60, from 1.14 to 0.63 and 6.88 to 0.93 respectively as a result of increasing temperature from 4 to 30°C. Furthermore, negative enthalpy ($\Delta H°$) and entropy ($\Delta S°$) changes were seen in adsorption of MB, FMTD and DFC on Ca-Alg2 and Ca-Alg2/GO beads (Table 1, 2 and 3). Negative enthalpy chance indicates that the adsorption processes is exothermic in nature while negative entropy change suggests a decrease of randomness at the solid-solute interface during adsorption [57]. Moreover, adsorption of MB and DFC on all beads was found to be spontaneous at 4°C and 22°C respectively due to negative Gibbs free energy changes ($\Delta G°$) however, spontaneity decreased to the increased temperature. The spontaneity was achieved when Ca-Alg_2/GO20 beads were used as adsorbent. Adsorption of FMDT on Ca-Alg_2/GO20 was only found to be spontaneous at 4 °C. Several studies indicate that the absolute magnitude of the change in Gibbs free energy for physisorption is between -20 kJ·mol^{-1} and 0 kJ·mol^{-1} and chemisorption occurs between -80 kJ·mol^{-1} and -400 kJ·mol^{-1} [58], [59]. Thus, adsorption process observed seems to be physisorption.

Preprints (www.preprints.org) | NOT PEER-REVIEWED | Posted: 24 September 2020 doi:10.20944/preprints202009.0562.v1

Table 1 Thermodynamic parameters for MB adsorption on Ca-Alg2, Ca-Alg2/GO5, Ca-Alg2/GO10 and Ca-Alg2/GO20 beads

Adsorbent	K_d			ΔG° [kJ·mol^{-1}]			ΔH° [kJ·mol^{-1}]	ΔS° [J·K^{-1}·mol^{-1}]
	4°C	22°C	30°C	4°C	22°C	30°C		
Ca-Alg$_2$	1.07	0.59	0.48	-0.144	1.240	1.855	-21.44	-76.9
Ca-Alg$_2$/GO5	1.18	0.77	0.73	-0.341	0.504	0.879	-13.34	-46.9
Ca-Alg$_2$/GO10	1.19	1.08	1.04	-0.401	-0.186	0.091	-3.712	-12.0
Ca-Alg$_2$/GO20	1.88	1.68	1.60	-1.459	-1.272	-1.189	-4.338	-10.4

Table 2 Thermodynamic parameters for FMTD adsorption on Ca-Alg2, Ca-Alg2/GO5, Ca-Alg2/GO10 and Ca-Alg2/GO20 beads

Adsorbent	K_d [-]			ΔG° [kJ·mol^{-1}]			ΔH° [kJ·mol^{-1}]	ΔS°[J·K^{-1}·mol^{-1}]
	4°C	22°C	30°C	4°C	22°C	30°C		
Ca-Alg$_2$	0.11	0.04	0.01	4.747	9.465	11.56	-67.85	-262
Ca-Alg$_2$/GO5	0.17	0.11	0.05	3.926	6.226	7.248	-31.46	-128
Ca-Alg$_2$/GO10	0.44	0.38	0.32	1.847	2.505	2.797	-8.277	-36.6
Ca-Alg$_2$/GO20	1.14	0.98	0.63	-0.418	0.473	0.868	-14.13	-49.5

Table 3 Thermodynamic parameters for DFC adsorption on Ca-Alg2, Ca-Alg2/GO5, Ca-Alg2/GO10 and Ca-Alg2/GO20 beads

Adsorbent	K_d [-]			ΔG° [kJ·mol^{-1}]			ΔH° [kJ·mol^{-1}]	ΔS° [J·K^{-1}·mol^{-1}]
	4°C	22°C	30°C	4°C	22°C	30°C		
Ca-Alg$_2$	2.90	1.55	0.55	-2.758	-0.042	1.165	-44.56	-151
Ca-Alg$_2$/GO5	4.96	1.80	0.58	-3.982	-0.704	0.753	-54.43	-182
Ca-Alg$_2$/GO10	5.48	2.61	0.74	-4.352	-1.342	-0.004	-50.67	-167
Ca-Alg$_2$/GO20	6.88	3.81	0.93	-4.896	-2.047	-0.781	-48.74	-158

Preprints (www.preprints.org) | NOT PEER-REVIEWED | Posted: 24 September 2020 doi:10.20944/preprints202009.0562.v1

3.4 Kinetics

Three models, Pseudo-first-order Lagergren, pseudo-second model and intraparticle diffusion, were fitted to the experimental data and the models are given in Figure 12. All the kinetic parameters for the adsorption of MB, FMTD and DFC are given in Table 4, 5 and 6.

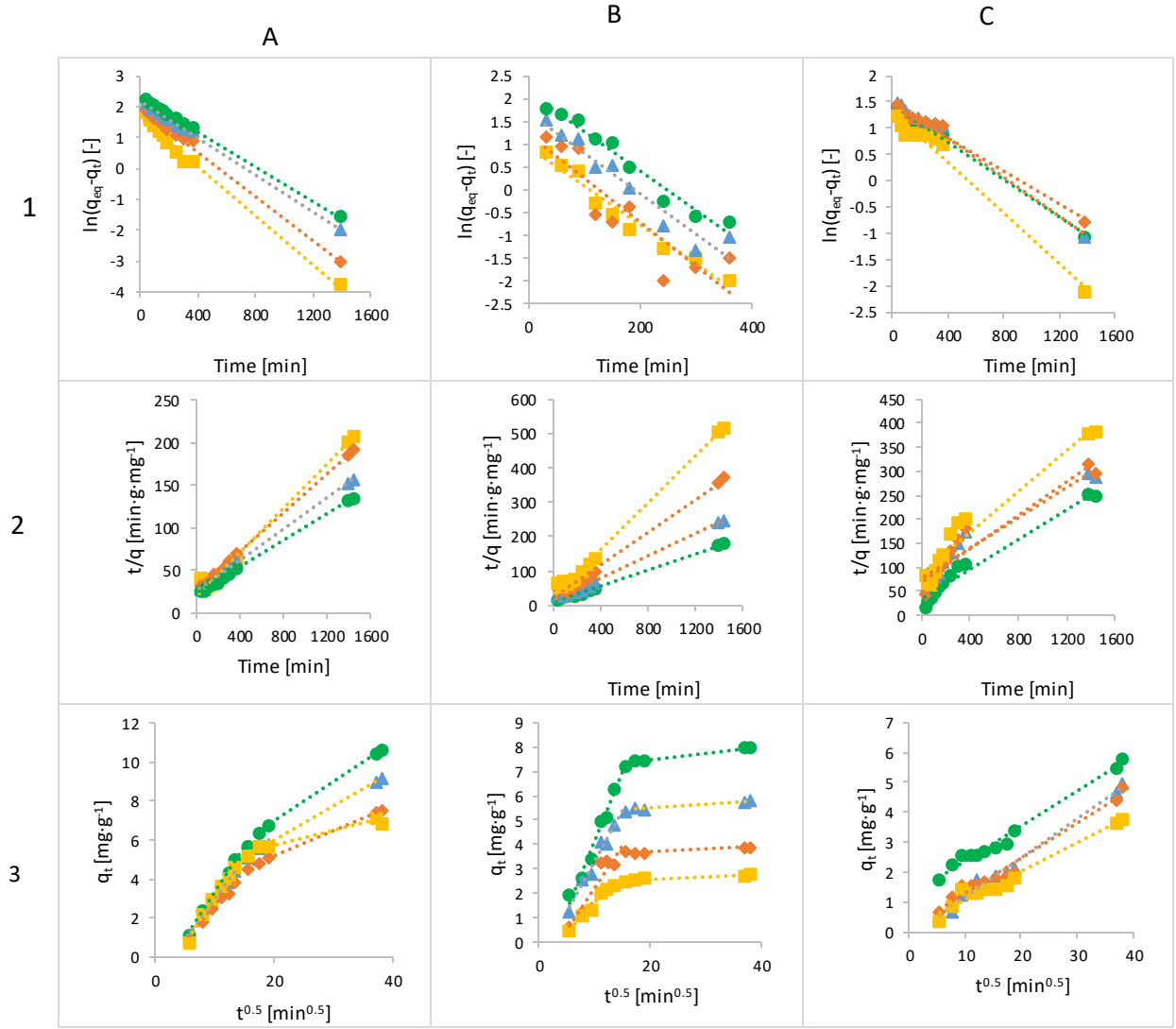

Figure 12 Linearized-integral form of the pseudo-first-order Lagergren equation of methylene blue (A1), famotidine (B1) and diclofenac (C1), linearized-integral form of the pseudo-second-order model of methylene blue (A2), famotidine (B2) and diclofenac (C2) and intraparticle diffusion model of methylene blue (A3), famotidine (B3) and diclofenac (C3) using Ca-Alg$_2$ (■), Ca-Alg$_2$/GO5 (♦), Ca-Alg$_2$/GO10 (▲) and Ca-Alg$_2$/GO20 (●) dried beads

Preprints (www.preprints.org) | NOT PEER-REVIEWED | Posted: 24 September 2020 doi:10.20944/preprints202009.0562.v1

Table 4 Kinetic parameters for MB adsorption onto Ca-Alg2, Ca-Alg2/GO5, Ca-Alg2/GO10 and Ca-Alg2/GO20 dried beads.

Adsorbent	Pseudo-first order			Pseudo-second order			Intraparticle diffusion					
	q_{eq} [mg g^{-1}]	k_1[min^{-1}]	R^2	q_{eq} [mg g^{-1}]	k_2 [g·mg^{-1}·min^{-1}]	R^2 [-]	$k_{id,1}$ [mg g^{-1}·min$^{-0.5}$]	C_1 [mg g^{-1}]	R^2	$k_{id,2}$ [mg g^{-1}·min$^{-0.5}$]	C_2 [mg g^{-1}]	R^2
Ca-Alg$_2$	6.27	$5.1\cdot10^{-3}$	0.9657	7.84	$8.3\cdot10^{-4}$	0.9907	0.479	-1.68	0.9875	0.0749	4.22	0.9580
Ca-Alg$_2$/GO5	7.22	$3.6\cdot10^{-3}$	0.9974	8.70	$5.0\cdot10^{-4}$	0.9995	0.358	-0.957	0.9950	0.128	2.69	0.9997
Ca-Alg$_2$/GO10	8.55	$3.0\cdot10^{-3}$	0.9979	10.81	$3.5\cdot10^{-4}$	0.9991	0.409	-1.10	0.9993	0.178	2.47	0.9996
Ca-Alg$_2$/GO20	9.79	$2.8\cdot10^{-3}$	0.9991	12.66	$2.7\cdot10^{-4}$	0.9993	0.457	-1.28	0.9958	0.202	2.94	0.9998

Table 5 Kinetic parameters for FMTD adsorption onto Ca-Alg2, Ca-Alg2/GO5, Ca-Alg2/GO10 and Ca-Alg2/GO20 dried beads

Adsorbent	Pseudo-first order			Pseudo-second order			Intraparticle diffusion					
	q_{eq} [mg g^{-1}]	k_1 [min^{-1}]	R^2	q_{eq} [mg g^{-1}]	k_2 [g·mg^{-1}·min^{-1}]	R^2	$k_{id,1}$ [mg g^{-1}·min$^{-0.5}$]	C_1 [mg g^{-1}]	R^2	$k_{id,2}$ [mg g^{-1}·min$^{-0.5}$]	C_2 [mg g^{-1}]	R^2
Ca-Alg$_2$	2.57	$8.6\cdot10^{-3}$	0.9597	2.93	$4.6\cdot10^{-3}$	0.9940	0.248	-0.882	0.9699	0.0098	2.39	0.8809
Ca-Alg$_2$/GO5	3.32	$9.5\cdot10^{-3}$	0.7828	4.15	$2.9\cdot10^{-3}$	0.9881	0.340	-1.23	0.8596	0.0116	3.44	0.9355
Ca-Alg$_2$/GO10	5.57	$9.0\cdot10^{-3}$	0.9315	6.06	$2.5\cdot10^{-3}$	0.9969	0.409	-0.821	0.9656	0.0137	5.23	0.8817
Ca-Alg$_2$/GO20	8.50	$8.6\cdot10^{-3}$	0.9631	8.50	$1.4\cdot10^{-3}$	0.9960	0.556	-1.44	0.9742	0.0271	6.93	0.9992

Table 6 Kinetic parameters for DFC adsorption onto Ca-Alg2, Ca-Alg2/GO5, Ca-Alg2/GO10 and Ca-Alg2/GO20 dried beads

Adsorbent	Pseudo-first order			Pseudo-second order			Intraparticle diffusion		
	q_{eq} [mg g^{-1}]	k_1 [min^{-1}]	R^2	q_{eq} [mg g^{-1}]	k_2 [g·mg^{-1}·min^{-1}]	R^2	k_{id} [mg g^{-1}·min$^{-0.5}$]	C [mg g^{-1}]	R^2
Ca-Alg$_2$	3.70	$2.4\cdot10^{-3}$	0.9756	4.64	$5.5\cdot10^{-4}$	0.9405	0.095	0.107	0.9684
Ca-Alg$_2$/GO5	4.28	$1.6\cdot10^{-3}$	0.9820	5.72	$4.4\cdot10^{-4}$	0.9147	0.117	0.110	0.9740
Ca-Alg$_2$/GO10	4.74	$1.9\cdot10^{-3}$	0.9865	6.31	$3.3\cdot10^{-4}$	0.9422	0.131	-0.130	0.9858
Ca-Alg$_2$/GO20	4.26	$1.8\cdot10^{-3}$	0.9879	6.33	$7.7\cdot10^{-4}$	0.9712	0.117	1.190	0.9835

Preprints (www.preprints.org) | NOT PEER-REVIEWED | Posted: 24 September 2020 doi:10.20944/preprints202009.0562.v1

The adsorbed amount of MB and FMTD predicted using the pseudo-first-order model are lower than the experimental data, and the values of R^2 are better for the pseudo-second-order. The experimental values for MB were 6.91mg g^{-1} and 10.63mg g^{-1} for Ca-Alg_2 and Ca-Alg_2/GO20 respectively, but the results for Pseudo-first-order were 6.27mg g^{-1} and 9.79mg g^{-1} for Ca-Alg_2 and Ca-Alg_2/GO20 respectively; for Pseudo second order the results were 7.84mg g^{-1} and 12.66mg g^{-1} higher than the experimental data, however the R^2 values are 0.9907 instead of 0.9657 for the case of Ca-Alg_2 or 0.9993 instead of 0.9991 for Ca-Alg_2/GO20. For FMTD the experimental results were 2.78 mg g^{-1} and 7.95mg g^{-1}, but the predictions for pseudo-first-order are 2.57 mg g^{-1} and 8.50 mg g^{-1} for Ca-Alg_2 and Ca-Alg_2/GO20 respectively; for pseudo-second-order the predictions were 2.93mg g^{-1} and 8.50mg g^{-1} as we can see the experimental data is higher than pseudo-first-order and lower than pseudo-second order only for the Ca-Alg_2 beads, for the Ca-Alg_2/GO20 beads the experimental results were lower than the predicted ones. However, the R^2 are better for the pseudo-second-order.

This indicates that the adsorption process does not fit the pseudo-first-order model, and shows applicability to the pseudo-second-order to describe the adsorption of methylene blue and famotidine onto Ca-Alg_2 and Ca-Alg_2/GO beads [60].

The diffusion mechanism during the adsorption process was studied using the intraparticle diffusion model. The plot of q_t versus $t^{1/2}$ shows a non-linear form indicating that the adsorption process occurs in more than one step as there is two distinct linear regions. The first straight region is attributed to the macro-pore diffusion and the second linear region to micro-pore diffusion. The first portion characterizes the instantaneous utilization of the adsorbing sites on the adsorbent surface. On the other hand, the second region is attributed to a slow diffusion of the methylene blue from the surface film into the micro-pores [61].

The predictions for the adsorbed amount of diclofenac obtained using the pseudo-first-order model fit the experimental data better than those obtained using the pseudo-second-order model. Experimental results were 3.78mg g^{-1} and 5.81mg g^{-1} for Ca-Alg_2 and Ca-Alg_2/GO20 respectively; for pseudo-first-order the predictions were 3.70mg g^{-1} and 4.64mg g^{-1} for Ca-Alg_2 and Ca-Alg_2/GO20 respectively; for pseudo-second-order the predictions were 4.26mg g^{-1} and 6.33mg g^{-1} for Ca-Alg_2 and Ca-Alg_2/GO20 respectively. The predictions are higher in every case except for pseudo-first-order and Ca-Alg_2/GO20 beads.

Preprints (www.preprints.org) | NOT PEER-REVIEWED | Posted: 24 September 2020 doi:10.20944/preprints202009.0562.v1

Moreover, the values of correlation coefficient R^2 are higher for the pseudo-first-order model meaning that the adsorption process of diclofenac into Ca-Alg_2 and Ca-Alg_2/GO beads can be described by the Largergren model. The intraparticle diffusion model shows a straight line indicating the adsorption process only because the intercept is close to 0 [62].

3.5 Adsorption Isotherms

The adsorption isotherms for methylene blue were built by testing nine different concentrations namely 1, 5, 10, 25, 50, 100, 250, 500 and 1000 $mg \cdot L^{-1}$. The adsorption was carried out over 24 hours at 125 rpm, room temperature and pH 7 with 0.05 g of beads. The isotherms obtained for each kind of beads are shown in Figure 13 and the data fit results are given in Table 7. The results obtained show that an increase in GO concentration of the beads improves the adsorbed amount of dye at equilibrium. The Langmuir model fits the experimental data better than the Freundlich model as indicated by goodness-of-fit tests (Table 7).

Preprints (www.preprints.org) | NOT PEER-REVIEWED | Posted: 24 September 2020 doi:10.20944/preprints202009.0562.v1

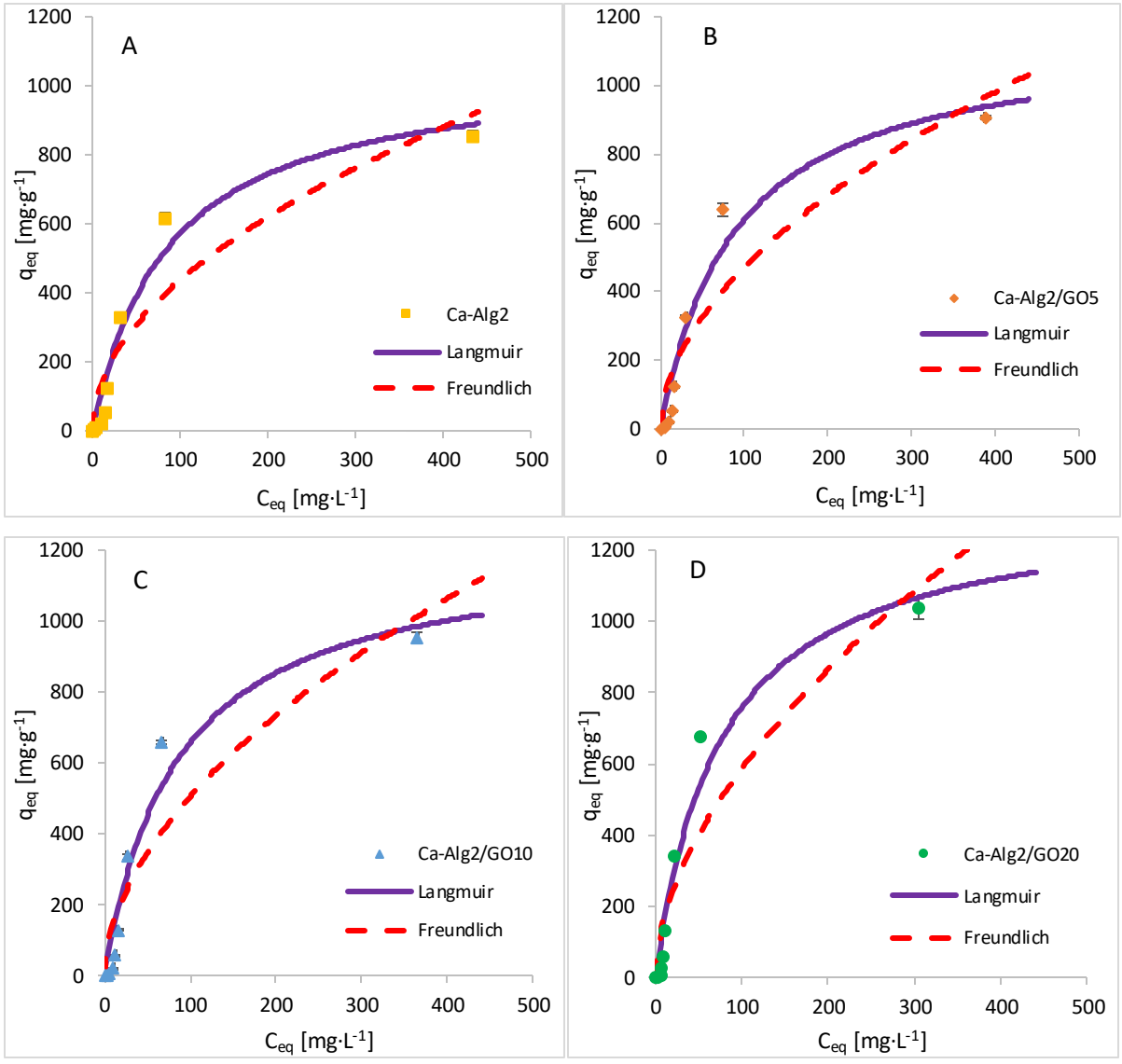

Figure 13 Adsorption isotherms for MB using A. Ca-Alg2, B. Ca-Alg2/GO5, C. Ca-Alg2/GO10 and D. Ca-Alg2/GO20 dried beads

Table 7 Langmuir and Freundlich isotherm constants for MB adsorption onto Ca-Alg_2 and Ca-Alg_2/GO beads

Adsorbent	Langmuir			Freundlich		
	q_{max} [mg·g^{-1}]	K_L [L·g^{-1}]	R^2 [-]	K_F[L·g^{-1}]	n [-]	R^2 [-]
Ca-Alg_2	1064	85.56	0.9778	43.26	0.503	0.9270
Ca-Alg_2/GO5	1153	88.93	0.9716	41.02	0.530	0.9109
Ca-Alg_2/GO10	1212	84.21	0.9782	42.64	0.537	0.8941
Ca-Alg_2/GO20	1334	76.21	0.9894	45.10	0.558	0.8541

Preprints (www.preprints.org) | NOT PEER-REVIEWED | Posted: 24 September 2020 doi:10.20944/preprints202009.0562.v1

The adsorption isotherms for FMTD were performed by using 1, 5, 10, 25, 50, 100 and 250 mgL^{-1} of solution whereas for diclofenac the concentrations were 1, 5, 10, 15 and 20 mgL^{-1}. The adsorption process was carried out over 24 hours at 125 rpm, room temperature and pH 7 with 0.05 g of beads. The adsorption models of FMTD and DFC are given in Figure 14 and Figure 15 while the data fit results are given in Table 8 and Table 9 respectively.

Table 8 Langmuir and Freundlich isotherm constants for FMTD adsorption onto Ca-Alg_2 and Ca-Alg_2/GO beads

Adsorbent	**Langmuir**			**Freundlich**		
	q_{max} [$mg \cdot g^{-1}$]	**K_L [$L \cdot g^{-1}$]**	**R^2 [-]**	**K_F [$L \cdot g^{-1}$]**	**n [-]**	**R^2 [-]**
Ca-Alg_2	28.96	123.2	0.9809	0.680	0.615	0.9351
Ca-Alg_2/GO5	31.69	85.39	0.9733	1.190	0.552	0.9173
Ca-Alg_2/GO10	33.57	57.02	0.9611	2.099	0.479	0.8593
Ca-Alg_2/GO20	35.50	23.10	0.9214	4.647	0.374	0.7491

Preprints (www.preprints.org) | NOT PEER-REVIEWED | Posted: 24 September 2020 doi:10.20944/preprints202009.0562.v1

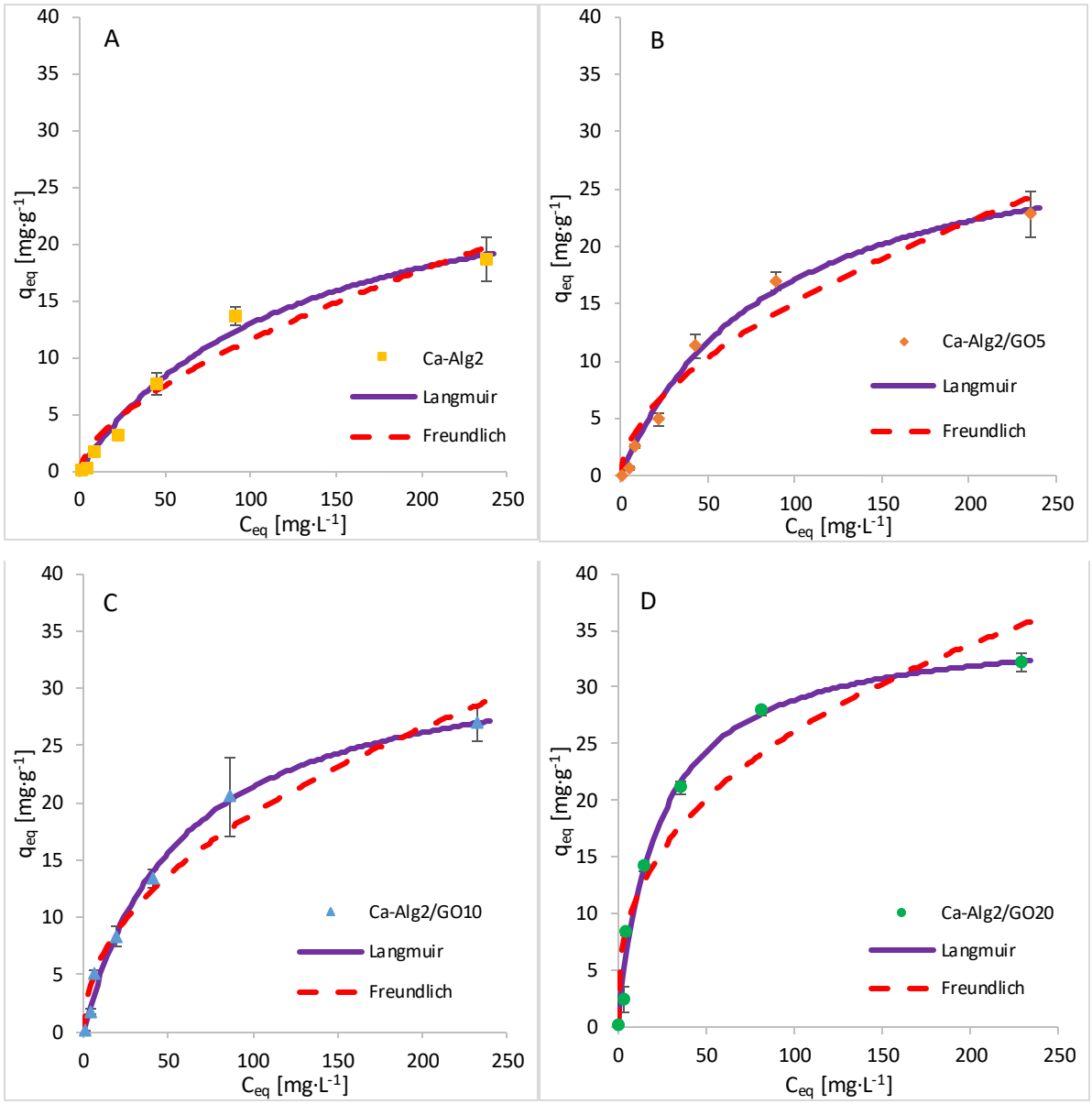

Figure 14 Adsorption isotherms of FMTD using A. Ca-Alg2, B. Ca-Alg2/GO5, C. Ca-Alg2/GO10 and D. Ca-Alg2/GO20 dried beads

Preprints (www.preprints.org) | NOT PEER-REVIEWED | Posted: 24 September 2020 doi:10.20944/preprints202009.0562.v1

Table 9 Langmuir and Freundlich isotherm constants for DFC adsorption onto Ca-Alg2 and Ca-Alg2/GO beads

Adsorbent	Langmuir			Freundlich		
	q_{max} [mg·g^{-1}]	K_L [L·g^{-1}]	R^2 [-]	K_F [L·g^{-1}]	n [-]	R^2 [-]
Ca-Alg$_2$	30.74	11.10	0.9457	2.795	0.725	0.8937
Ca-Alg$_2$/GO5	31.81	9.020	0.9175	3.441	0.705	0.8707
Ca-Alg$_2$/GO10	33.72	5.988	0.8886	5.055	0.662	0.8401
Ca-Alg$_2$/GO20	36.35	5.066	0.8872	5.992	0.672	0.8322

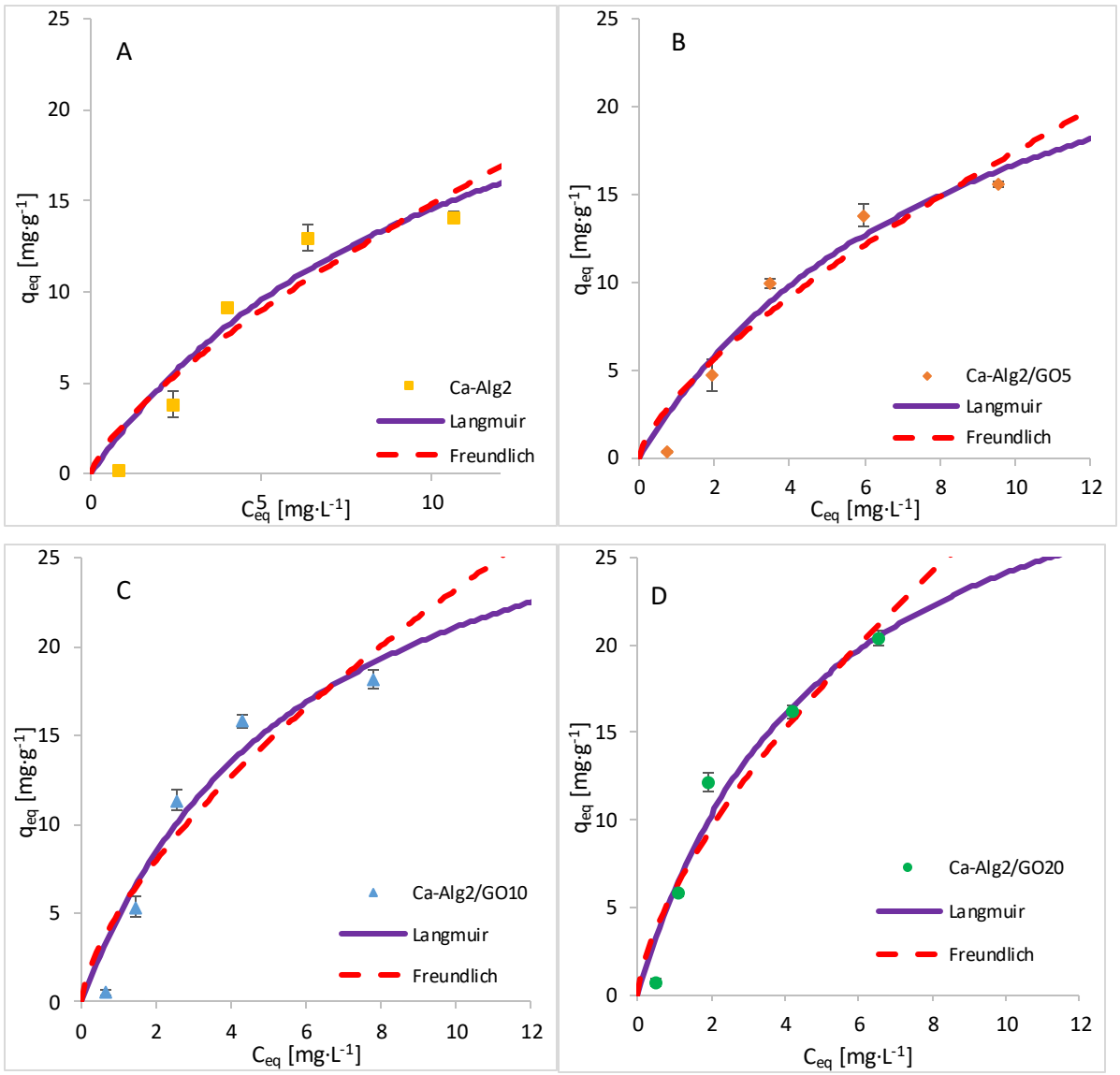

Figure 15 Adsorption isotherms of DFC using A. Ca-Alg2, B. Ca-Alg2/GO5, C. Ca-Alg2/GO10 and d. Ca-Alg2/GO20 dried beads

The results for the adsorption isotherms of FMTD and DFC indicate similar behaviour than MB. Indeed, the Langmuir model fits better the experimental data for each compound with

Preprints (www.preprints.org) | NOT PEER-REVIEWED | Posted: 24 September 2020 doi:10.20944/preprints202009.0562.v1

every different kind of beads. Table 7, 8 and 9 shows the Langmuir and Freundlich isotherm constants and correlation coefficients for MB, FMTD and DFC adsorption.

The values of R^2 are higher with Langmuir model indicating that this model fits better the experimental data than the Freundlich isotherm for each kind of beads and each pharmaceutical. The Langmuir model supposes that the adsorption process occurs on a homogenous surface by monolayer adsorption.

Constants K_F and n indicate the adsorption capacity and the adsorption intensity respectively. As indicated by the experimental data, the adsorption capacity K_F is increasing gradually with graphene oxide concentration and constant n is lower than 1 meaning the adsorption isotherm is favourable. Maximum adsorption capacities q_{max} obtained are 1334, 35, 50 and 36.35 mg g^{-1} for the uptake of methylene blue, famotidine and diclofenac respectively. It means that Ca-Alg_2/GO beads are an efficient adsorbent for the removal of these contaminants, particularly for methylene blue as, to our knowledge, this is the highest adsorption capacity for MB that been reported in the literature.

3.6 Desorption

The desorption of each compound adsorbed onto Ca-Alg2 and Ca-Alg2/GO beads was studied by using HCl/NaOH 0.1M, NaCl 1M and ethanol 1% v:v. The results of the percentage desorbed after 24 hours are shown in Figure 17.

Preprints (www.preprints.org) | NOT PEER-REVIEWED | Posted: 24 September 2020 doi:10.20944/preprints202009.0562.v1

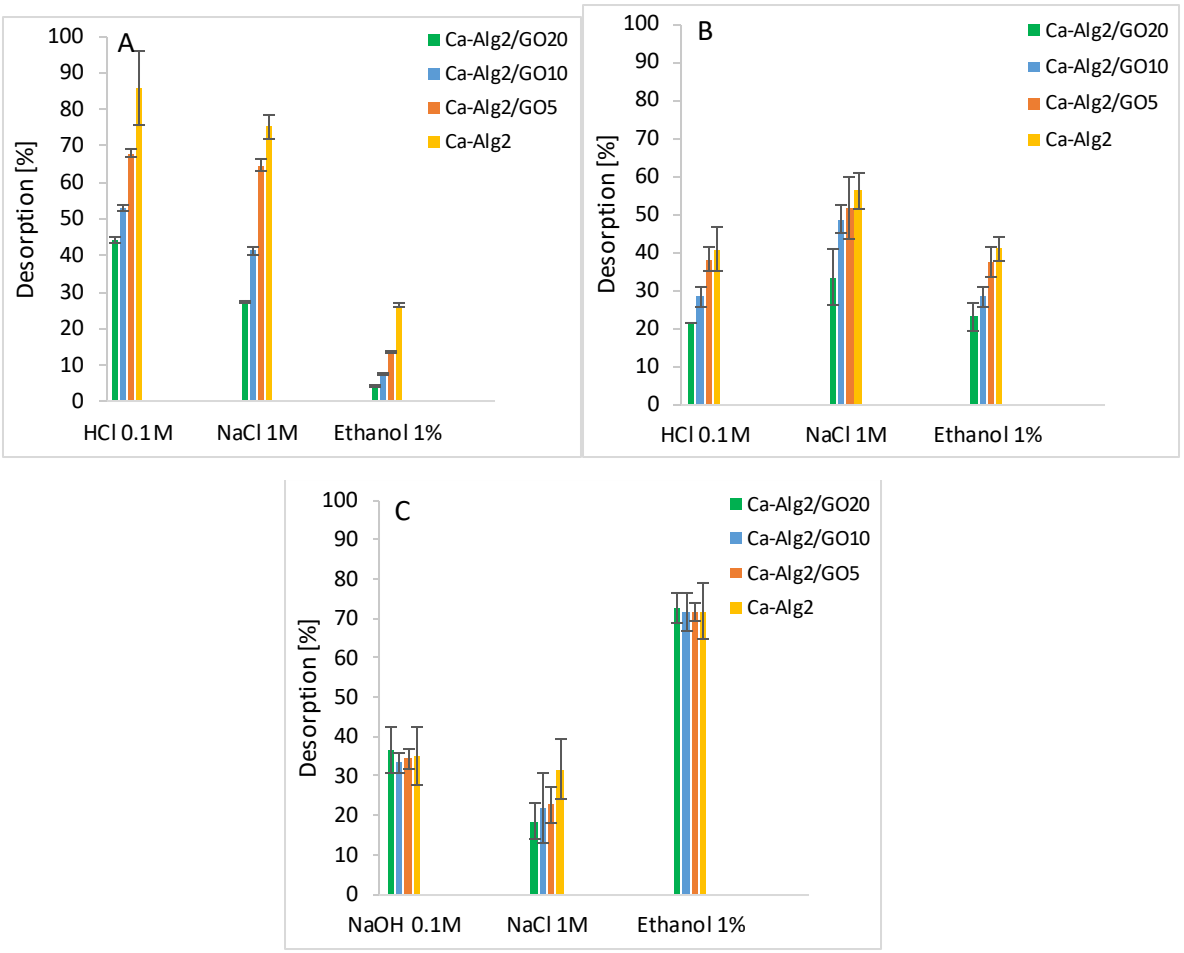

Figure 16 Desorption [%] of A. MB, B. FMTD and C. DFC

The desorption of MB from the beads was higher when using HCl 0.1 M than with NaCl or ethanol. The results showed that 89 ± 9.9 % and 44 ± 0.6 % of MB are desorbed for Ca-Alg_2 and Ca-Alg_2/GO20 beads respectively. Indeed, protons H^+ in excess seem able to force the cationic dye to be released by taking place on the adsorption sites on the surface of the beads. It is more difficult to effect release of MB from beads with graphene oxide due to a stronger affinity. NaCl 1 M also showed good results for the desorption of MB. However, the ionic strength of sodium chloride 1 M destabilizes the structure of calcium alginate beads, making them soft, fragile and crumbly. As such, high concentration salt solution cannot be use as a desorbent due to the inability to reuse the beads. Ethanol solution showed little desorption of MB as the main interactions between adsorbate and adsorbent are typically ionic bonds and ethanol has little effect to remove the dye from the beads with van der Waals' forces.

On the other hand, the desorption of famotidine using HCl 0.1 M showed less satisfactory results. It might be due to a poor solubility at low pH solution or due to hydrogen bonds between the adsorbent and the adsorbate making hydrochloric acid unable to release the

Preprints (www.preprints.org) | NOT PEER-REVIEWED | Posted: 24 September 2020 doi:10.20944/preprints202009.0562.v1

drug into the solution. Hydrogen bonds could also explain why the ionic strength of NaCl is also inefficient to remove the cationic pharmaceutical from the beads in addition to destroying the stability of the beads. As for MB, ethanol has little effect with van der Waals' interaction for the removal of famotidine because of the stability of hydrogen bonds.

The results for the desorption of diclofenac from the beads showed that ethanol 1% v:v is able to release the pharmaceutical into solution. The percentages of desorption are high, around 70%, and the results present little difference between each kind of beads. Diclofenac was desorbed with NaOH 0.1 M from the beads mainly due to a change in the pH of the solution. As the results of the effect of pH showed, the adsorption of diclofenac was low in high pH solution. Like the other compounds, NaCl is not an efficient desorbent and damages the stability of the beads by interacting with the structure of the polymer.

4 Conclusions

The SEM analysis showed that an increase in graphene oxide modified the morphological structure of the beads. Indeed, they become more porous and rougher with a higher surface available for the interactions between adsorbate and adsorbent. As expected, during the adsorption process, Ca-Alg_2/GO20 beads present the best adsorption for each compound. The effect of initial concentration, adsorbent dose, pH and temperature all play an important role for the adsorption. The results show that a higher concentration of pharmaceuticals increases the diffusion driving force of drug adsorbed by the beads. With a lower concentration of beads, the adsorbed amount at equilibrium q_{eq} increases because of a higher amount adsorbed per unit of weight of the adsorbent. On the other hand, the percentage of removal decreases due to less adsorption sites available. The pH can modify the structure of the beads along with the pharmaceuticals causing a change in the interactions between adsorbate and adsorbent. The adsorption process is better at low temperature than high temperature meaning the adsorption mechanism is exothermic (as confirmed by H°) and thermodynamic studies show that the physisorption is spontaneous. The pseudo-second order model is the best fit to the experimental data concerning the kinetics of adsorption for methylene blue and famotidine, however the Lagergren pseudo-first order model suits better for diclofenac. Furthermore, each compound follows the Langmuir model for the isotherm adsorption with a maximum adsorption capacity of 1334, 35.50 and 36.35 $mg \cdot g^{-1}$ for methylene blue, famotidine and diclofenac, respectively. It should be noted that the adsorption capacity of

Preprints (www.preprints.org) | NOT PEER-REVIEWED | Posted: 24 September 2020 doi:10.20944/preprints202009.0562.v1

MB onto calcium alginate graphene oxide beads, particularly Ca-Alg_2/GO20 composites, was found to be superior in comparison to other adsorbents ranging from commercial activated carbon (980.3 $mg \cdot g^{-1}$) to bioadsorbents such as modified biomass of baker's yeast (869.6 $mg \cdot g^{-1}$) along with many other natural adsorbents, biomass and coal derived activate carbon as reviewed in detail by [63]. In addition, GO and alginate incorporation outperformed recently published graphene derived nanocomposite (Fe_3O_4-graphene at mesoporous SiO_2) where the adsorption capacity was reported to be 178.49 $mg \cdot g^{-1}$ in terms of MB removal [32]. Furthermore, in the adsorption capacity of MB was recently published as 150.66 $mg \cdot g^{-1}$ when GO was incorporated with sodium alginate to produce aero gel beads Therefore, it concluded that graphene oxide calcium alginate composite is a superabsorbent for MB removal from water in addition to being superior to the previously published researches [41], [64]. Furthermore, by treating the Alg_2/GO20 composites that had come in contact with the absorbates MB or diclofenac with 0.1 M HCl and ethanol 1% v:v the absorbates could be efficiently removed/desorbed and the Alg_2/GO20 composite beads were regenerated without damage to bead integrity. Further investigation needs to be performed for famotidine as little desorption is observed with the desorption candidates examined.

These beads appear to be an efficient adsorbent for dyes and pharmaceuticals, particularly for methylene blue. This novel technology could be applied as a polishing step in water treatment in order to reduce the concentration of these micro-pollutants as well as the synthetic dyes which negatively impact the environment, human health and aquatic life. Methylene Blue is widely used a model pollutant in adsorption studies. It is interesting to note that while the performance of the beads assessed in this study is excellent for MB, it is less than stellar for FMTD and DFC. This calls into question the validity of the common approach of single component pollutant for novel adsorbent testing.

 doi:10.20944/preprints202009.0562.v1

Acknowledgements

The authors gratefully acknowledge the Environmental Protection Agency grant 2011-W-MS-8 for financial support for Declan McGlade and Alexander Yavorskyy, and the support of the Erasmus+ programme of the European Union for undergraduate student mobility.

Disclaimer: The European Commission support for the production of this publication does not constitute an endorsement of the contents which reflects the views only of the authors, and the Commission cannot be held responsible for any use which may be made of the information contained therein.

References

[1] Y. Luo *et al.*, "A review on the occurrence of micropollutants in the aquatic environment and their fate and removal during wastewater treatment.," *Sci. Total Environ.*, vol. 473–474, pp. 619–41, Mar. 2014, doi: 10.1016/j.scitotenv.2013.12.065.

[2] J. Z. Guo, B. Li, L. Liu, and K. Lv, "Removal of methylene blue from aqueous solutions by chemically modified bamboo," *Chemosphere*, vol. 111, pp. 225–231, 2014, doi: 10.1016/j.chemosphere.2014.03.118.

[3] F. Benstoem *et al.*, "Elimination of micropollutants by activated carbon produced from fibers taken from wastewater screenings using hydrothermal carbonization," *J. Environ. Manage.*, vol. 211, pp. 278–286, 2018, doi: 10.1016/j.jenvman.2018.01.065.

[4] M. G. Anderson *et al.*, "The Challenge of Micropollutants," *Sci. Technol.*, no. August, pp. 1072–1077, 2006, doi: 10.1126/science.1127291.

[5] T. H. Miller, N. R. Bury, S. F. Owen, J. I. MacRae, and L. P. Barron, "A review of the pharmaceutical exposome in aquatic fauna," *Environ. Pollut.*, vol. 239, pp. 129–146, Aug. 2018, doi: 10.1016/J.ENVPOL.2018.04.012.

[6] Y. S. Jeon, J. Lei, and J. H. Kim, "Dye adsorption characteristics of alginate/polyaspartate hydrogels," *J. Ind. Eng. Chem.*, vol. 14, no. 6, pp. 726–731, 2008, doi: 10.1016/j.jiec.2008.07.007.

[7] O. Keskinkan and M. Z. L. Göksu, "Assessment of the dye removal capability of submersed aquatic plants in a laboratory-scale wetland system using ANOVA," *Brazilian J. Chem. Eng.*, vol. 24, no. 2, pp. 193–202, 2007, doi: 10.1590/S0104-66322007000200004.

[8] A. K. Mittal, "Stdie or Soretio of Dycr by Sulfomlcd Col dA Gamdema fucidutn," no. April 1989, 2014.

[9] E. N. El Qada, S. J. Allen, and G. M. Walker, "Adsorption of Methylene Blue onto activated carbon produced from steam activated bituminous coal: A study of equilibrium adsorption isotherm," *Chem. Eng. J.*, vol. 124, no. 1–3, pp. 103–110, 2006, doi: 10.1016/j.cej.2006.08.015.

[10] Y. Bulut and H. Aydin, "A kinetics and thermodynamics study of methylene blue adsorption on wheat shells," *Desalination*, vol. 194, no. 1–3, pp. 259–267, 2006, doi: 10.1016/j.desal.2005.10.032.

[11] A. F. Hassan, A. M. Abdel-Mohsen, and M. M. G. Fouda, "Comparative study of

calcium alginate, activated carbon, and their composite beads on methylene blue adsorption," *Carbohydr. Polym.*, vol. 102, no. 1, pp. 192–198, 2014, doi: 10.1016/j.carbpol.2013.10.104.

[12] S. Y. Lin, "An overview of famotidine polymorphs: Solid-state characteristics, thermodynamics, polymorphic transformation and quality control," *Pharm. Res.*, vol. 31, no. 7, pp. 1619–1631, 2014, doi: 10.1007/s11095-014-1323-5.

[13] L. A. Kristofco and B. W. Brooks, "Global scanning of antihistamines in the environment: Analysis of occurrence and hazards in aquatic systems," *Sci. Total Environ.*, vol. 592, pp. 477–487, 2017, doi: 10.1016/j.scitotenv.2017.03.120.

[14] S. Murphy, C. Saurel, A. Morrissey, J. Tobin, M. Oelgemöller, and K. Nolan, "Photocatalytic activity of a porphyrin/TiO 2 composite in the degradation of pharmaceuticals," *Appl. Catal. B Environ.*, vol. 119–120, pp. 156–165, May 2012, doi: 10.1016/j.apcatb.2012.02.027.

[15] T. S. Rad, A. Khataee, B. Kayan, D. Kalderis, and S. Akay, "Synthesis of pumice-TiO2 nanoflakes for sonocatalytic degradation of famotidine," *J. Clean. Prod.*, vol. 202, pp. 853–862, Nov. 2018, doi: 10.1016/j.jclepro.2018.08.165.

[16] R. Bort, X. Ponsoda, R. Jover, M. J. Gómez-Lechón, and J. V Castell, "Diclofenac toxicity to hepatocytes: a role for drug metabolism in cell toxicity.," *J. Pharmacol. Exp. Ther.*, vol. 288, no. 1, pp. 65–72, 1999.

[17] P. McGettigan and D. Henry, "Cardiovascular Risk and Inhibition of Cyclooxygenase," *Jama*, vol. 296, no. 13, p. 1633, 2006, doi: 10.1001/jama.296.13.jrv60011.

[18] M. Gros, M. Petrović, A. Ginebreda, and D. Barceló, "Removal of pharmaceuticals during wastewater treatment and environmental risk assessment using hazard indexes," *Environ. Int.*, vol. 36, no. 1, pp. 15–26, 2010, doi: 10.1016/j.envint.2009.09.002.

[19] R. Triebskorn, H. Casper, V. Scheil, and J. Schwaiger, "Ultrastructural effects of pharmaceuticals (carbamazepine, clofibric acid, metoprolol, diclofenac) in rainbow trout (Oncorhynchus mykiss) and common carp (Cyprinus carpio)," *Anal. Bioanal. Chem.*, vol. 387, no. 4, pp. 1405–1416, 2007, doi: 10.1007/s00216-006-1033-x.

[20] K. Nambirajan, S. Muralidharan, A. A. Roy, and S. Manonmani, "Residues of Diclofenac in Tissues of Vultures in India: A Post-ban Scenario," *Arch. Environ. Contam. Toxicol.*, vol. 74, no. 2, pp. 292–297, Feb. 2018, doi: 10.1007/s00244-017-

0480-z.

[21] G. Starukh, "Photocatalytically Enhanced Cationic Dye Removal with Zn-Al Layered Double Hydroxides," *Nanoscale Res. Lett.*, vol. 12, 2017, doi: 10.1186/s11671-017-2173-y.

[22] R. Huang *et al.*, "Fabrication and Adsorption Behavior of Magnesium Silicate Hydrate Nanoparticles towards Methylene Blue," *Nanomaterials*, vol. 8, no. 5, p. 271, 2018, doi: 10.3390/nano8050271.

[23] S. Basha *et al.*, "UV-induced photocatalytic degradation of aqueous acetaminophen: the role of adsorption and reaction kinetics," *Environ. Sci. Pollut. Res.*, vol. 22, no. 3, 2015, doi: 10.1007/s11356-014-3411-9.

[24] L. Zhao, S. T. Yang, S. Feng, Q. Ma, X. Peng, and D. Wu, "Preparation and application of carboxylated graphene oxide sponge in dye removal," *Int. J. Environ. Res. Public Health*, vol. 14, no. 11, 2017, doi: 10.3390/ijerph14111301.

[25] D. L. Cunha, A. Kuznetsov, C. A. Achete, A. E. da H. Machado, and M. Marques, "Immobilized TiO_2 on glass spheres applied to heterogeneous photocatalysis: photoactivity, leaching and regeneration process," *PeerJ*, vol. 6, p. e4464, 2018, doi: 10.7717/peerj.4464.

[26] Z. Feng, K. Odelius, G. K. Rajarao, and M. Hakkarainen, "Microwave carbonized cellulose for trace pharmaceutical adsorption," *Chem. Eng. J.*, vol. 346, pp. 557–566, Aug. 2018, doi: 10.1016/j.cej.2018.04.014.

[27] L. Lin, W. Jiang, and P. Xu, "Comparative study on pharmaceuticals adsorption in reclaimed water desalination concentrate using biochar: Impact of salts and organic matter," *Sci. Total Environ.*, vol. 601–602, pp. 857–864, Dec. 2017, doi: 10.1016/j.scitotenv.2017.05.203.

[28] O. Paunovic, S. Pap, S. Maletic, M. A. Taggart, N. Boskovic, and M. Turk Sekulic, "Ionisable emerging pharmaceutical adsorption onto microwave functionalised biochar derived from novel lignocellulosic waste biomass," *J. Colloid Interface Sci.*, vol. 547, pp. 350–360, Jul. 2019, doi: 10.1016/j.jcis.2019.04.011.

[29] D. Shan *et al.*, "Preparation of ultrafine magnetic biochar and activated carbon for pharmaceutical adsorption and subsequent degradation by ball milling," *J. Hazard. Mater.*, vol. 305, pp. 156–163, Mar. 2016, doi: 10.1016/j.jhazmat.2015.11.047.

[30] Y. Yan, J. Li, F. Kong, K. Jia, S. He, and B. Wang, "L-Lysine-grafted graphene oxide as an

effective adsorbent for the removal of methylene blue and metal ions," *Beilstein J. Nanotechnol.*, vol. 8, no. 1, pp. 2680–2688, 2017, doi: 10.3762/bjnano.8.268.

[31] M. A. Khan, B. H. Hameed, J. Lawler, M. Kumar, and B. H. Jeon, "Developments in activated functionalized carbons and their applications in water decontamination: a review," *Desalin. Water Treat.*, vol. 54, no. 2, 2015, doi: 10.1080/19443994.2014.885397.

[32] X. L. Wu, Y. Shi, S. Zhong, H. Lin, and J. R. Chen, "Facile synthesis of Fe 3 O 4 - graphene@mesoporous SiO 2 nanocomposites for efficient removal of Methylene Blue," *Appl. Surf. Sci.*, vol. 378, pp. 80–86, 2016, doi: 10.1016/j.apsusc.2016.03.226.

[33] S. Wu *et al.*, "Adsorption properties of doxorubicin hydrochloride onto graphene oxide: Equilibrium, kinetic and thermodynamic studies," *Materials (Basel).*, vol. 6, no. 5, pp. 2026–2042, 2013, doi: 10.3390/ma6052026.

[34] X. Deng, L. Lü, H. Li, and F. Luo, "The adsorption properties of Pb(II) and Cd(II) on functionalized graphene prepared by electrolysis method," *J. Hazard. Mater.*, vol. 183, no. 1–3, pp. 923–930, 2010, doi: 10.1016/j.jhazmat.2010.07.117.

[35] E. Repo, J. K. Warchoł, A. Bhatnagar, and M. Sillanpää, "Heavy metals adsorption by novel EDTA-modified chitosan-silica hybrid materials," *J. Colloid Interface Sci.*, vol. 358, no. 1, pp. 261–267, 2011, doi: 10.1016/j.jcis.2011.02.059.

[36] K. Kadirvelu, K. Thamaraiselvi, and C. Namasivayam, "Removal of heavy metals from industrial wastewaters by adsorption onto activated carbon prepared from an agricultural solid waste," *Bioresour. Technol.*, vol. 76, no. 1, pp. 63–65, 2001, doi: 10.1016/S0960-8524(00)00072-9.

[37] W. M. Algothmi, N. M. Bandaru, Y. Yu, J. G. Shapter, and A. V. Ellis, "Alginate-graphene oxide hybrid gel beads: An efficient copper adsorbent material," *J. Colloid Interface Sci.*, vol. 397, pp. 32–38, 2013, doi: 10.1016/j.jcis.2013.01.051.

[38] T. Chandy, D. L. Mooradian, and G. H. R. Rao, "Evaluation of modified alginate-chitosan-polyethylene glycol microcapsules for cell encapsulation," *Artif. Organs*, vol. 23, no. 10, pp. 894–903, 1999, doi: 10.1046/j.1525-1594.1999.06244.x.

[39] D. Dutta, B. J. Borah, L. Saikia, M. G. Pathak, P. Sengupta, and D. K. Dutta, "Synthesis and catalytic activity of Ni°-acid activated montmorillonite nanoparticles," *Appl. Clay Sci.*, vol. 53, no. 4, pp. 650–656, 2011, doi: 10.1016/j.clay.2011.05.018.

[40] A. A. Oladipo and M. Gazi, "Enhanced removal of crystal violet by low cost

alginate/acid activated bentonite composite beads: Optimization and modelling using non-linear regression technique," *J. Water Process Eng.*, vol. 2, pp. 43–52, 2014, doi: 10.1016/j.jwpe.2014.04.007.

[41] T. E, D. Ma, S. Yang, and X. Hao, "Graphene oxide-montmorillonite/sodium alginate aerogel beads for selective adsorption of methylene blue in wastewater," *J. Alloys Compd.*, vol. 832, p. 154833, 2020, doi: 10.1016/j.jallcom.2020.154833.

[42] M. Kumar, D. McGlade, M. Ulbricht, and J. Lawler, "Quaternized polysulfone and graphene oxide nanosheet derived low fouling novel positively charged hybrid ultrafiltration membranes for protein separation," vol. 5, no. 63, pp. 51208–51219, 2015.

[43] M. Zhou, Q. Li, S. Zhong, J. Chen, H. Lin, and X. L. Wu, "Facile large scale fabrication of magnetic carbon nano-onions for efficient removal of bisphenol A," *Mater. Chem. Phys.*, vol. 198, pp. 186–192, 2017, doi: 10.1016/j.matchemphys.2017.05.020.

[44] S. J. Allen, G. McKay, and J. F. Porter, "Adsorption isotherm models for basic dye adsorption by peat in single and binary component systems," *J. Colloid Interface Sci.*, vol. 280, no. 2, pp. 322–333, 2004, doi: 10.1016/j.jcis.2004.08.078.

[45] T. Liu *et al.*, "Adsorption of methylene blue from aqueous solution by graphene," *Colloids Surfaces B Biointerfaces*, vol. 90, pp. 197–203, 2012, doi: 10.1016/j.colsurfb.2011.10.019.

[46] Y. Li *et al.*, "Removal of copper from aqueous solution by carbon nanotube/calcium alginate composites," *J. Hazard. Mater.*, vol. 177, no. 1–3, pp. 876–880, 2010, doi: 10.1016/j.jhazmat.2009.12.114.

[47] S. R. Popuri, Y. Vijaya, V. M. Boddu, and K. Abburi, "Adsorptive removal of copper and nickel ions from water using chitosan coated PVC beads," *Bioresour. Technol.*, vol. 100, no. 1, pp. 194–199, 2009, doi: 10.1016/j.biortech.2008.05.041.

[48] B. H. Hameed, "Evaluation of papaya seeds as a novel non-conventional low-cost adsorbent for removal of methylene blue," *J. Hazard. Mater.*, vol. 162, no. 2–3, pp. 939–944, 2009, doi: 10.1016/j.jhazmat.2008.05.120.

[49] N. M., Islam, M., "Solubility , Stability and Ionization Behaviour of Farnotidine," *J. Pharm. Sci.*, vol. 45, no. 8, pp. 682–686, 1993.

[50] B. Konkena and S. Vasudevan, "Understanding Aqueous Dispersibility of Graphene Oxide and Reduced Graphene Oxide through p K," *Phys. Chem. Lett.*, 2012, doi:

10.1021/jz300236w.

[51] N. L. Francis *et al.*, "An ice-templated , linearly aligned chitosan-alginate scaffold for neural tissue engineering," *J. Biomed. Mater. Res. Part A*, vol. 101, no. 12, pp. 3493–3503, 2013, doi: 10.1002/jbm.a.34668.

[52] V. Rocher, J. M. Siaugue, V. Cabuil, and A. Bee, "Removal of organic dyes by magnetic alginate beads," *Water Res.*, vol. 42, no. 4–5, pp. 1290–1298, 2008, doi: 10.1016/j.watres.2007.09.024.

[53] F. J. Beltrán, P. Pocostales, P. Alvarez, and A. Oropesa, "Diclofenac removal from water with ozone and activated carbon," *J. Hazard. Mater.*, vol. 163, no. 2–3, pp. 768–776, 2009, doi: 10.1016/j.jhazmat.2008.07.033.

[54] S. W. Nam *et al.*, "Adsorption characteristics of diclofenac and sulfamethoxazole to graphene oxide in aqueous solution," *Chemosphere*, vol. 136, pp. 20–26, 2015, doi: 10.1016/j.chemosphere.2015.03.061.

[55] Y. Li *et al.*, "Methylene blue adsorption on graphene oxide/calcium alginate composites," *Carbohydr. Polym.*, vol. 95, no. 1, pp. 501–507, 2013, doi: 10.1016/j.carbpol.2013.01.094.

[56] Y. S. Al-Degs, M. I. El-Barghouthi, A. H. El-Sheikh, and G. M. Walker, "Effect of solution pH, ionic strength, and temperature on adsorption behavior of reactive dyes on activated carbon," *Dye. Pigment.*, vol. 77, no. 1, pp. 16–23, 2008, doi: 10.1016/j.dyepig.2007.03.001.

[57] M. Kumar, B. P. Tripathi, and V. K. Shahi, "Crosslinked chitosan/polyvinyl alcohol blend beads for removal and recovery of Cd(II) from wastewater," *J. Hazard. Mater.*, vol. 172, no. 2–3, pp. 1041–1048, 2009, doi: 10.1016/j.jhazmat.2009.07.108.

[58] C. H. Weng, Y. T. Lin, and T. W. Tzeng, "Removal of methylene blue from aqueous solution by adsorption onto pineapple leaf powder," *J. Hazard. Mater.*, vol. 170, no. 1, pp. 417–424, 2009, doi: 10.1016/j.jhazmat.2009.04.080.

[59] S. S. Han and H. M. Lee, "Adsorption properties of hydrogen on (10,0) single-walled carbon nanotube through density functional theory," *Carbon N. Y.*, vol. 42, no. 11, pp. 2169–2177, 2004, doi: 10.1016/j.carbon.2004.04.025.

[60] P. Wang, M. Cao, C. Wang, Y. Ao, J. Hou, and J. Qian, "Kinetics and thermodynamics of adsorption of methylene blue by a magnetic graphene-carbon nanotube composite," *Appl. Surf. Sci.*, vol. 290, pp. 116–124, 2014, doi: 10.1016/j.apsusc.2013.11.010.

[61] M. Doğan, Y. Özdemir, and M. Alkan, "Adsorption kinetics and mechanism of cationic methyl violet and methylene blue dyes onto sepiolite," *Dye. Pigment.*, vol. 75, no. 3, pp. 701–713, 2007, doi: 10.1016/j.dyepig.2006.07.023.

[62] W. H. Cheung, Y. S. Szeto, and G. McKay, "Intraparticle diffusion processes during acid dye adsorption onto chitosan," *Bioresour. Technol.*, vol. 98, no. 15, pp. 2897–2904, 2007, doi: 10.1016/j.biortech.2006.09.045.

[63] M. Rafatullah, O. Sulaiman, R. Hashim, and A. Ahmad, "Adsorption of methylene blue on low-cost adsorbents: A review," *J. Hazard. Mater.*, vol. 177, no. 1–3, pp. 70–80, 2010, doi: 10.1016/j.jhazmat.2009.12.047.

[64] S. A. Ali, I. Y. Yaagoob, M. A. J. Mazumder, and H. A. Al-Muallem, "Fast removal of methylene blue and Hg(II) from aqueous solution using a novel super-adsorbent containing residues of glycine and maleic acid," *J. Hazard. Mater.*, vol. 369, no. February, pp. 642–654, 2019, doi: 10.1016/j.jhazmat.2019.02.082.